Simulation and Flow Characterization of Spiked Supersonic Gas Turbine Intake at Non-Zero Angle of Attack

by

Tan Kien Weng

Dissertation submitted in partial fulfilment of

the requirements for the

Bachelor of Engineering (Hons)

(Mechanical Engineering)

JUNE 2009

Universiti Teknologi PETRONAS

Bandar Seri Iskandar

31750 Tronoh

Perak Darul Ridzuan

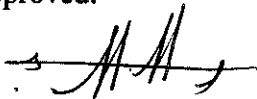# CERTIFICATION OF APPROVAL

SIMULATION AND FLOW CHARACTERIZATION OF SPIKED SUPERSONIC GAS TURBINE INTAKE AT NON-ZERO ANGLE OF ATTACK

by

Tan Kien Weng

A project dissertation submitted to the
Mechanical Engineering Programme
Universiti Teknologi PETRONAS
in partial fulfilment of the requirement for the
Bachelor of Engineering (Hons)
(Mechanical Engineering)

Approved:

_____
AP. Dr. Hussain Al-Kayiem
Project Supervisor

UNIVERSITI TEKNOLOGI PETRONAS
TRONOH, PERAK

June 2009

CERTIFICATION OF ORIGINALITY

This is to certify that I am responsible for the work submitted in this project, that the original work is my own except as specified in the references and acknowledgements, and that the original work contained herein have not been undertaken or done by unspecified sources or persons.

TAN KIEN WENG

ABSTRACT

Intake of a supersonic gas turbine requires the highest possible total pressure recovery and minimal total pressure lost in order to obtain an efficient operation. The supersonic intake is mainly affected by two substantial factors which are the angle of attack and the geometry of the spike (wedge angle). At zero angle of attack, the solution is quite direct, but at non-zero angle of attack, the shock system structure will be affected and the flow distribution will be unsymmetrical in the upper (leeside) and the lower side (windward side) of the inlet. The objective of this work is to analyze the thermo fluid mechanism and to investigate the flow characteristic in the diffuser part of the intake. The analysis is carried out under the assumption of viscous, steady, 2D compressible fluid flow. The external part (shock system part) is to be modelled and analyzed analytically. The shock system part is successfully modelled using Microsoft Excel. The internal part (diffuser) will be simulated and analyzed numerically using CFD software. The available FLUENT and GAMBIT software in the department will be used for modelling and simulation. In conclusion, the study on combination effect of angle of attack and wedge angle is very essential as it directly affect the performance of the compressor and in turn, the gas turbine operation.

ACKNOWLEDGEMENT

First and foremost, I would like to extend my gratitude to the Almighty God for His abundant love and faithfulness. The project will never come to a completion without the support, hard work and endless effort by a large number of individuals. Hence, I would like to take this golden opportunity to thank each and every one of them.

My heartfelt gratitude is specially dedicated to my project supervisor AP Dr. Hussain Al-Kayiem for his excellent guidance and advices. I would like to thank him for his dedication of time and effort, relentless teaching and motivation towards the completion of my final year project. Besides, his confidences over me by giving me numerous of challenging tasks, have given me abundance of learning opportunities.

Besides, I would also like to express my appreciation to the lecturers that had made time to attend numerous presentations on this project and had never cease to provide their advice in hope of achieving the objectives. Not forgetting, to my fellow course mates that had helped in guiding me throughout the progress of this project.

Last but not least, I would also like to thank express my love and thanks to my family members for their understanding, support, love and encouragement throughout this period.

TABLE OF CONTENT

List of Figures

List of Tables

NOMENCLATURE

Symbol

a	Local speed of sound
C_p	Specific heat at constant pressure for air
D_H	Hydraulic diameter
H	Altitude of aircraft
k	Thermal conductivity
L	Length of diffuser
M	Mach no.
P	Pressure
P_o	Stagnation Pressure
R	Gas constant
Re	Reynolds number
T	Temperature
u	Velocity component in X-direction
v	Velocity component in Y-direction
V	Velocity in one-dimensional flow
w	Width of the diffuser
X, Y	Cartesian coordinates
y	Height of diffuser
α	Angle of attack(incident angle)
δ	Deflection(wedge) angle
δ_{max}	Maximum deflection(wedge) angle
γ	Specific hear ratio, for air(1.4)
μ	Viscosity coefficient
θ	Optimum angle
ρ	Density
σ	Oblique shock angle
σ_{max}	Maximum oblique shock angle
υ	Prandtl-Meyer shock angle

Subscript

1	Upstream of the shock
2	Downstream of the shock
x	Upstream of the N.S.W
y	Downstream of the N.S.W
∞	Free Stream

Abbreviations

CFD	Computational fluid dynamics
N.S.W	Normal shock waves
O.S.W	Oblique shock wave
P-M	Prandtl-Mayer wave

CHAPTER 1

INTRODUCTION

The title of this research is Simulation and Flow Characterization of Spiked Supersonic Gas Turbine at Non-Zero Angle of Attack. In this section, a brief introduction on the supersonic gas intake will be discussed. The problem statement, objectives, scope of study and significant of work will be covered as well.

1.1 BACKGROUND

The designs of the inlet of the supersonic gas turbine engines play a vital role in determining the performance of the propulsion system of an aircraft. At present, all turbojet engines require subsonic flow at the entry of the compressor face where it must be reduced to approximately 0.3 to 0.5 Mach, even if the aircraft is flying at supersonic speed. However, in decelerating the external supersonic flow to a subsonic speed acceptable to the compressor, there will be pressure losses which will highly affect the performance of the gas turbine. Therefore, the intake has to be properly designed to reduce the velocity of the air intake and simultaneously keep the total pressure losses to a minimum.

Basically an intake of a supersonic gas turbine consists of two main parts which is the spike and the subsonic diffuser shown in Figure 1. [1]
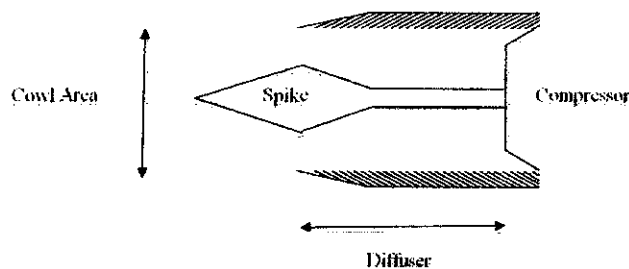
Figure 1.1: Simple Intake.

1.2 PROBLEM STATEMENT

In supersonic gas turbine engines, the shock wave system and air mass flow rate are controlled by spiked intake. Non zero incidence angle changes the effective deflection angle of the shock wave at the upper and the lower side of the spike, so the combining effect of incidence and forebody angles is essential for the intake performance of the gas turbine engine.

1.3 OBJECTIVES

The objectives of this research are:
- To simulate numerically the spiked intake of supersonic gas turbine engine.
- To analyse the thermo fluid mechanism and investigate the flow characteristics in the diffuser part of the intake at different angle of attack.

1.4 SCOPE OF STUDY

In this research, there are three scope of studies required. First, is the modelling of the external and internal part of the supersonic intake. The modelling of the external part will be modelled using programming Microsoft Excel whereas the internal part will be modelled using CFD software.

Secondly, is to investigate the pressure distribution in the diffuser part by performing a simulation on the spiked intake of supersonic gas turbine. The results from the simulation are to be verified by comparing with similar numerical works and experimental works.

Thirdly, is to perform a simulation and analysis of the spiked supersonic intake at different angle of attack and Mach number.

1.5   SIGNIFICANT OF THE WORK

High efficiency and performance of a supersonic gas turbine engine is one of the most important criteria for a turbojet engine. With the change of incidence and forebody angle, the pressure distribution of the diffuser part in the leeside and the windward side will be highly affected. The difference in pressure distribution in the leeside and windward side will hence affect the performance of air compression in the gas turbine engine. In addition, if the difference in pressure distribution between the two sides of the compressor is too high, it will also cause mechanical failure, for example the bending of the compressor blade and bearing failure.

The present research is to investigate the pressure distribution and the flow characteristic at the diffuser part of the intake at higher accuracy so that in the future, further modification can be done on the intake to improve the efficiency of the gas turbine or to provide information to the operator on the unfavourable region of the operation for continuous safety flight. In addition, the reliability of the gas turbine engine can be increased with the avoidance of mechanical failure.

CHAPTER 2

LITERATURE REVIEW

A spike is a wedge or cone-shaped body which is positioned at the gas turbine intake with the main purpose of creating shock series outside the intake front face. The spike installed in the gas turbine can be a stationary and a movable spike. For the stationary spike, the geometry is fixed and hence leads to a fixed throat area. On the other hand, the movable spikes will provide a variable geometry intake. This kind of intake are required to produce a throat area which is large enough for the establishment of supersonic flow and, which can subsequently be reduced to provide efficient wedge compression in the running conditions. [2]

With the use of spike, the deceleration of the flow intake from supersonic to subsonic are conducted in stages instead of just a single step (as by only with the normal shock wave). [3] With the implementation of spike at the inlet, two types of shock waves will be created, which is the oblique shock wave and the normal shock wave. The number of oblique shock wave is determined by geometry of the spike (number of corners or the contour of the spike).
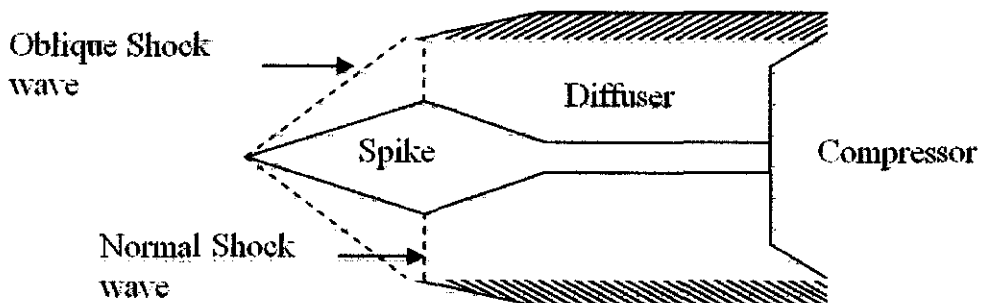
Figure 2.1: Supersonic Spiked Intake with One Deflection Feature.

The operational characteristics of an oblique shock diffuser can be summarized into three typical conditions which are the critical, subcritical and supercritical modes. The critical operation mode is denoted when the normal shock wave is exactly at the position of the diffuser throat, where the cross section is minimal. Hence, the airflow rate is at maximum and stagnation pressure losses are minimal.

If the normal shock waves moves upstream the duct entry, then this intake mode of operation is denoted as subcritical, as shown is Figure 3(b). [4] This condition is highly unstable and will produce shock oscillating in high rate at the intake. As if the normal shock moves downstream the throat, it will results in poor flow quality. This intake operation is denoted as supercritical, as shown in Figure 3(c).
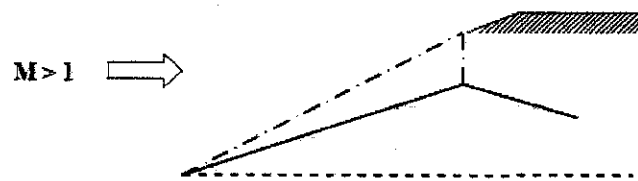
(a) Critical
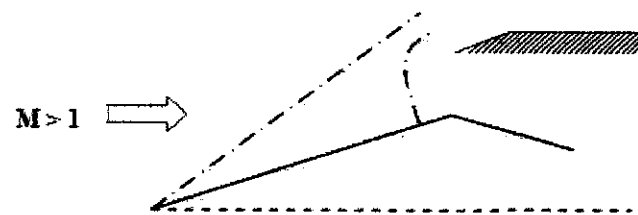
(b) Subcritical
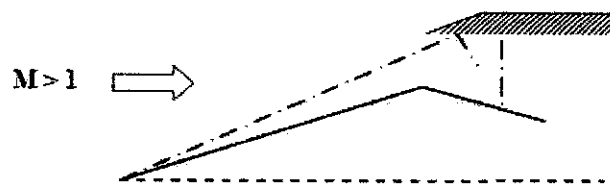
(c) Supercritical

Figure 2.2: Supersonic Intake-Modes of Operation.

The intake performance of the supersonic gas turbine engines are basically affected by two substantial factors which are:

- The angle of attack (α) and
- The spike geometry (forebody angle (δ) and shape of spike).

At different angle of attack, the upper side (lee side) and the lower side (windward side) will experience different shock system. When the angle of attack is larger than zero, the oblique shock wave on the lee side will possessed smaller shock angle and experience supercritical condition. Whereas in the windward side, the deflection angle of the shock wave is larger and consequently, the variation of properties is larger than in the lee side. [5]

Figure 2.3: Outline of Two-Dimensional Inlets.

2.1 LITERATURE SURVEY

Beastall(1953) presented the certain types of flow instability that occur with the centre-body diffuser at supersonic speed. An experimental work has been suggested to provide data in 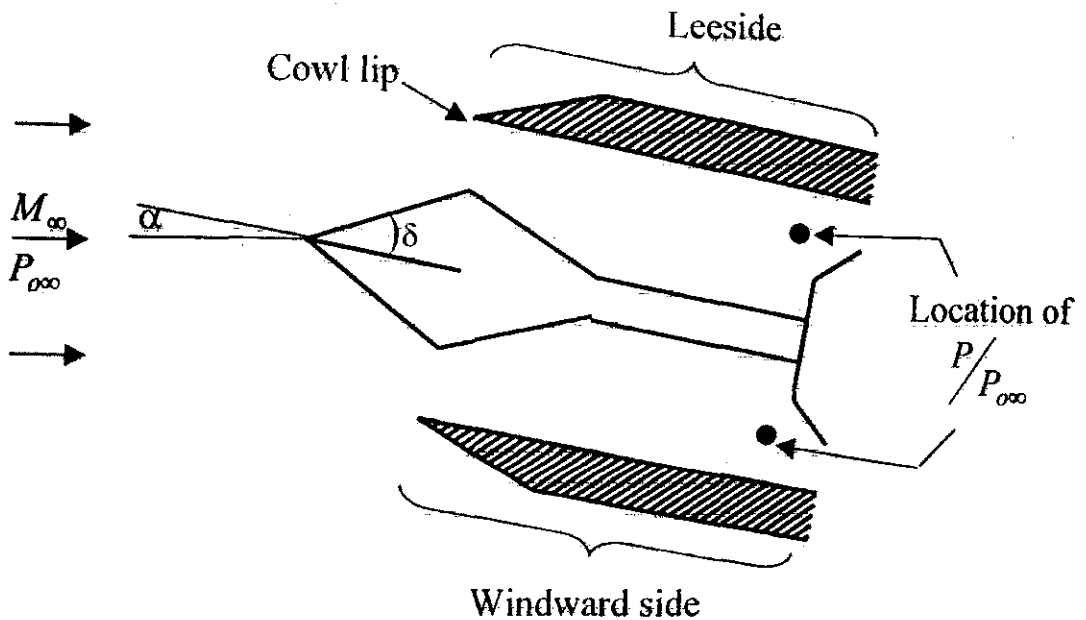designing diffuser which are stable with regards to large and small oscillation. Experimental work suggested that wind tunnel test should be done with different wedge angle and different position of centre-body with a given Mach number. Limits of position of centre body for unstable flow can be found and hence with this information it is possible to design a diffuser which is stable. Further testing are still required as although a diffuser may be stable with regards to large oscillation it may still be vulnerable to small oscillation.[6]

2001, S.S Gokhale and V.R.Kumar uses the compressible Navier-Stokes equations in two dimensions without body force or external heat addition as the governing equation. The Baldwin-Lomax turbulence model is used to simulate the effects of fine scale turbulence. A Prandtl-Van Driest formulation is used in the inner region and the Clauser formulation with Klebanoff intermittence function is used in the outer region.

A 151*91 grid with clustering near the wall region is used to predict the pressure in the duct region. For Scramjet, the inlet Mach of 3.0 and 2.5 with same geometry is considered in the study. From the isoMach contour plot it show for both Mach no, the flow in the duct is shock free as only isentropic compression takes place followed by compression due to cowl shock impinging on the lower wall.

The code created is capable of predicting all complex inlet flow features(shock due to forebody, multiple shock reflections, normal shock, shock boundary layer interaction and associated separation for two dimensional and axisymmetric inlets and computed values are in good agreement with the experimental data available. The code can be used to study supersonic inlet performance under off-design operating conditions. [7]

7

Salih (2003) carried out an analysis on the effect of angle of attack on the shock system in the single wedge and double wedge spikes to the pressure recovery in the inlet of compressor. The analysis is carried out by dividing the intake into two parts; the external part (the shock wave system) and the internal (subsonic diffuser). The external part (shock wave system) is modelled and analysed analytically. The flow in the subsonic diffuser part is considered perfect, non-viscous and two dimensional. The set of governing equation is to be solved by Patankar method called "SIMPLE". A preliminary program was design to state the inlet boundary conditions by taking into account the shock system at the inlet of intake Study was done on the pressure recovery behaviour with the change in angle of attack(from 0 to 10) at different flying Mach numbers(1.8 and 2.2) for single wedge and double wedge spike($\delta_1 = 6^o, \delta_2 = 4^o, \beta = 6^o$).

The flow assumption of viscous flow is necessary to be taken into consideration as different results are obtained than that of non-viscous flow assumption. The results obtained from the numerical analysis are in agreement with those obtained experimentally by previous researchers. [5]

In *2003, Thangadurai and Chandra* solved governing equations and boundary conditions are using the flow simulation software FLUENT. Finer grids were used in the steep-gradient zones, such as boundary layers near the walls and also at the locations of normal and oblique shocks. The conservation equations for mass, momentum, energy and turbulence quantities are solved using the finite volume technique. The results from the numerical analysis are then validated by comparing with the experimental data.

Axisymmetric and two-dimensional supersonic mixed compression air intake of realistic configuration has been studied. For axisymmetric mixed compression, the predicted cowl inner wall static pressure and pressure recovery show good agreement with the experimental data. As for the two-dimensional mixed compression, the prediction of static pressure variation along the cowl inner surface and the ramp outer surface show good agreement with the experimental data as well.

From the results of the numerical simulation also, heat addition significantly increases the pressure recovery along the cowl inner surface and centre body. The model developed by the author to predict the flow in air intake is able to capture the flow features such as shock pattern and pressure recovery. The flow model developed can be used effectively to predict the flow environment in generic intake. [8]

Jain and Mittal (2005) carried out a numerical simulation of 2D mixed compression supersonic inlet by solving unsteady compressible Euler equation via a stabilized finite element method.

Computations are carried out for various back pressures with the same inlet geometry (R52.1" configuration) ranging from 20 to 32.4. As the back pressure increases the normal shock wave moves to the convergent part. When it is increased till 32.4, the normal shock wave moves ahead of the throat and causes unstart.

Computations also done on four different geometries: inlet where they have air intakes with different length of the second ramp. All intakes have the same total length and throat area. The four geometries of inlet are denoted by R54.5, R54.1, R53.3 and R52.1(R54.4 means 54.4" from the leading edge of intake till the throat).From the results, the last main reflected oblique shock from the cowl surface lies in the convergent section for the R54.5 and R54.1 cases and in the divergent section for the other two geometries. Hence, unstart occurs for R54.5 and R54.1.

Critical pressure and corresponding total pressure recovery is higher for inviscid flow. The variation between total pressure recovery and back pressure is almost linear. As the back pressure increases the normal shock waves moves upstream towards throat where pressure losses decreases. It is found that in addition to the throat-to- inlet area ration, the ramp geometries plays an important role in the start-up dynamics.[9]

Al-Kayiem & Aboud (2007) carried out an analysis of the flow field in the supersonic spike intake by subdivided it into three different region. The first and second regions which are the flow across oblique shock wave and across normal shock wave are predicted by analytical simulation using the related governing equations. The equations are solved under different operating condition and results after the normal shock wave is used as inlet conditions for the internal part of intake. The internal part of intake is analysed by CFD technique based on finite difference approximation. The solution is carried out numerically under assumption of 2-D, compressible and non-viscous. The nodal network was re-mapped by using a rectangular computational nodal network to represents the complex physical domain

The results are obtained for different operating condition at incidence angles=$0^o,4^o,8^o,12^o,16^o$ and 20°. Mach number is varied from 1.3 to 3. The entire analysis is carried out with two different spike deflection angles (6° and 12°). The total pressure recovery is the main parameter for comparison at different conditions.

From the results the total pressure recovery evaluation demonstrates considerable variation in the pressure forces at the compressor inlet. The angle of attack and spike angle contributes effectively in the flow structure and resulting in pressure recovery in the compressor inlet. [4]

Soltani et. al (2008) studied the effect of heat source addition to the performance improvement of a supersonic external compression. Firstly, he solved the flow field around the inlet without heat addition by using commercial CFD code. The numerical solver uses a hybrid grid with triangular and quadrilateral cells. The numerical results were then compared with the experimental data. This is done to validate the numerical prediction. After the comparison is done, the effect of heat addition was investigated in two methods. First method is by heating the front portion of spike .The second method is by placing a heat source at a distance away from the body. The effect of heat source position on the flow field was investigated. After finding the best location, the optimum size and shape is obtained using try and error method.

Results show that from the first method, the drag coefficient is reduced. However, it reduces the inlet mass flow significantly. In the second method, the heat source always reduces the drag coefficient but in some locations it may reduce the inlet efficiency and mass flow rate. The best location was found which is in front of the spike nose not very far from the nose oblique shock. In this location, the drag coefficient reduces significantly and inlet efficiency and inlet mass flow increased negligibly. It is also found that the best shape of heat source was a rectangular cross section that stretched in the free stream flow direction. The second method is a more suitable method to use as if it is placed in a suitable position the drag coefficient can be reduced and mass flow rate and inlet efficiency can be increased.[10]
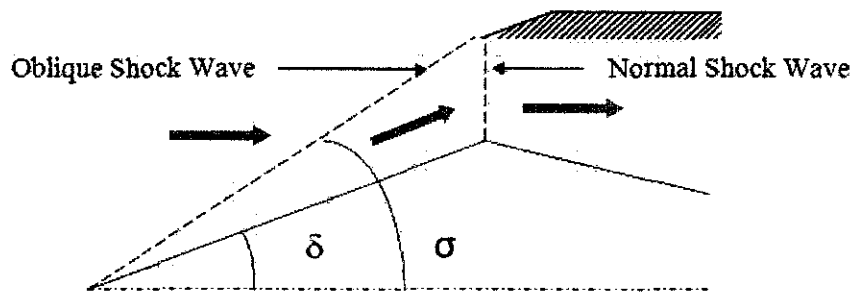
CHAPTER 3

THEORY OF COMPRESSIBLE FLUID FLOW

Figure 3.1: Shock Waves in the Intake.

The following assumptions are being used in this study:

1. The fluid is perfect, i.e

Constant pressure specific heat, Cp	= 1.005 kJ/kg.K
Specific heat ratio, γ	= 1.4
Gas constant, R	= 0.287 kJ/kg.K

Since the flow is compressible, i.e. density not constant, and it can be evaluated from the equation of state as shown below:

$$\rho = \frac{P}{RT} \quad (3.1)$$

and velocity at any point is equal to:

$$V = Ma \quad (3.2)$$

where

$$a = \sqrt{\gamma RT} \quad (3.3)$$

2. The flow is isentropic through the external flow except through the layer of shock which is adiabatic.

3. The flow field in the diffuser part is considered as 2-D, steady and viscous (μ= constant).

4. The spike is of fixed geometry, i.e. the critical condition cannot be achieved every time

5. Free stream properties (T∞, P∞) depend on the altitude of the aircraft(H)[for this study the fly is assumed at 10000m] as in these relations: [5]

$$T\infty = 288.16 - 0.0065H \qquad (3.4)$$

$$P_\infty = 101325(\frac{T_\infty}{288.16})^{\frac{0.03415H}{288.16 - T_\infty}} \qquad (3.5)$$

3.1 MODELLING OF SHOCK SYSTEM

3.1.1 Isentropic Flow

The isentropic flow is characterized by frictionless and adiabatic flow. As in this study, the local Mach number is the reference or characteristic parameter. When the flow area is changed, the velocity would change. With the change of velocity the Mach number along the stream wise would change as well. As a result, the local flow properties would change and are evaluated in the ratio form as shown below [5]:-

Pressure ratio:

$$\frac{p_0}{p} = [1 + \frac{\gamma - 1}{2}M^2]^{\frac{\gamma}{\gamma - 1}} \qquad (3.6a)$$

Density ratio:

$$\frac{\rho_0}{\rho} = [1 + \frac{\gamma - 1}{2}M^2]^{\frac{1}{\gamma - 1}} \qquad (3.6b)$$

Temperature ratio:

$$\frac{T_o}{T} = \left[1 + \frac{\gamma - 1}{2} M^2 \right] \qquad (3.6c)$$

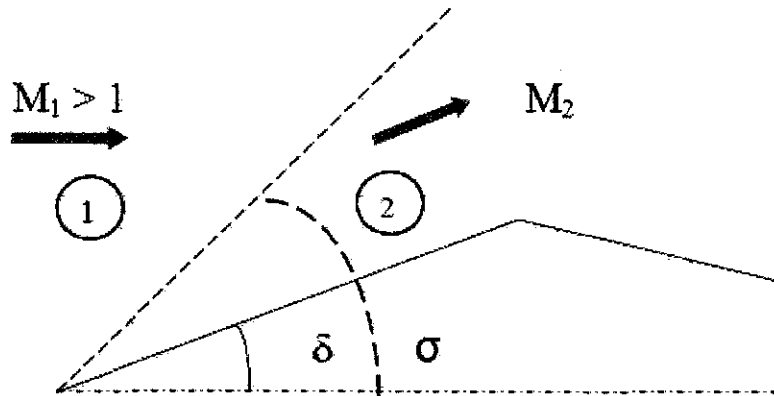### 3.1.2 Modelling of Oblique Shock Wave

Figure 3.2: Oblique Shock Wave.

The properties of flow behind the oblique shock wave is function of the upstream Mach number, assume M_1, and the shock angle (σ) can be found by equation below using iterative solution.

$$\tan\delta = \frac{2 \cot\sigma \, (M_1^2 \sin^2\sigma - 1)}{2 + M_1^2 (\gamma + \cos2\sigma)} \qquad (3.7a)$$

Downstream Mach number

$$M_2 = \sqrt{\frac{(\gamma - 1)M_1^2 \sin^2\sigma + 2}{2\gamma M_1^2 \sin^2\sigma - (\gamma - 1)\sin^2\sigma} \cdot \frac{1}{\sin^2(\sigma - \delta)}} \qquad (3.7b)$$

Pressure ratio

$$\frac{P_2}{P_1} = \frac{2\gamma}{\gamma + 1} M_1^2 \sin^2\sigma - \frac{\gamma - 1}{\gamma + 1} \qquad (3.7c)$$

14

Density ratio:

$$\frac{\rho_2}{\rho_1} = \frac{(\gamma + 1)M_1^2 sin^2 \sigma}{2 + (\gamma - 1)M_1^2 sin^2 \sigma} \qquad (3.7d)$$

Temperature ratio

$$\frac{T_2}{T_1} = \left(\frac{2\gamma}{\gamma + 1}M_1^2 sin^2 \sigma - \frac{\gamma - 1}{\gamma + 1}\right)\left(\frac{2 + (\gamma - 1)M_1^2 sin^2 \sigma}{(\gamma + 1)M_1^2 sin^2 \sigma}\right) \qquad (3.7e)$$

Total pressure ratio

$$\frac{Po_2}{Po_1} = \frac{P_2}{P_1}\left(\frac{1 + \frac{\gamma - 1}{2}M_2^2}{1 + \frac{\gamma - 1}{2}M_1^2}\right)^{\frac{\gamma}{\gamma - 1}} \qquad (3.7f)$$

3.1.3 Modelling of Normal Shock Wave

M > 1 P_x P_y M < 1

           ρ_x ⇨   ⇨ ρ_y

           T_x T_y

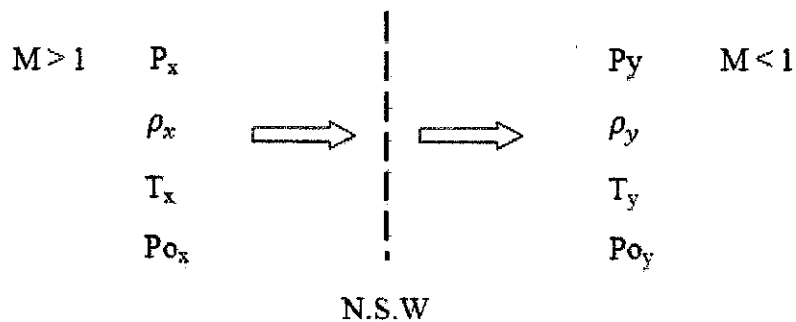 Po_x Po_y

N.S.W

Figure 3.3: Normal Shock Wave.

The upstream of the shock is defined as (x) and the downstream behind the normal shock wave is denoted by (y).

Downstream Mach number

$$M_y = \sqrt{\frac{(\gamma - 1)M_x^2 + 2}{2\gamma M_x^2 - (\gamma - 1)}} \qquad (3.8a)$$

Pressure ratio

$$\frac{P_y}{P_x} = \frac{2\gamma}{\gamma+1}M_x^2 - \frac{\gamma-1}{\gamma+1} \qquad (3.8b)$$

Density Ratio

$$\frac{\rho_y}{\rho_x} = \frac{(\gamma+1)M_x^2}{2+(\gamma-1)M_x^2} \qquad (3.8c)$$

Temperature ratio

$$\frac{T_y}{T_x} = \left(\frac{2\gamma}{\gamma+1}M_x^2 - \frac{\gamma-1}{\gamma+1}\right)\left(\frac{2+(\gamma-1)M_x^2}{(\gamma+1)M_x^2}\right) \qquad (3.8d)$$

Total pressure ratio

$$\frac{Po_y}{Po_x} = \left(\frac{2\gamma}{\gamma+1}M_x^2 - \frac{\gamma-1}{\gamma+1}\right)^{\frac{-1}{\gamma-1}}\left(\frac{(\gamma+1)M_x^2}{2+(\gamma-1)M_x^2}\right)^{\frac{\gamma}{\gamma-1}} \qquad (3.8e)$$
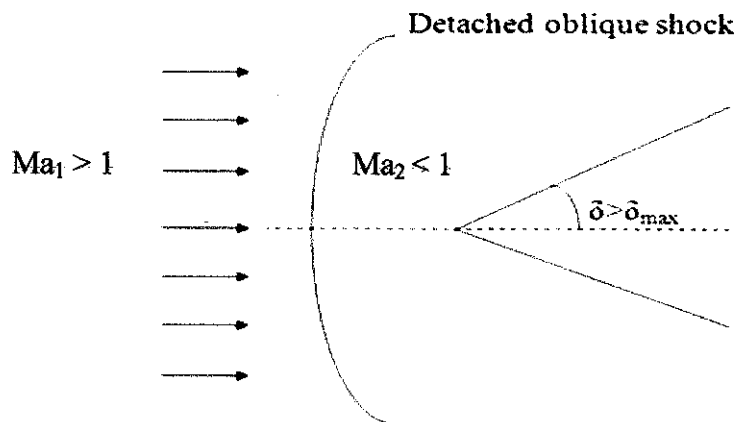
3.1.4 Modelling of Detached Shock Wave

Figure 3.4: Detached Shock Wave.

16

Detached shock wave is shock waves with no contact with the body it originates from. It occurs, when the flow pass a wedge with deflection angle greater than maximum deflection angle for detail Mach number i.e. when $\delta > \delta_{max}$

δ_{max} can be found from the equation:

$$\tan \delta_{max} = \frac{2 \cot \sigma_{max} (M_1 sin^2 \sigma_{max} - 1)}{2 + M_1^2 (\gamma + cos2\sigma_{max})} \qquad (3.9a)$$

Where σ_{max} is obtained from:

$$sin^2 \sigma_{max} = \frac{\gamma + 1}{4\gamma} - \frac{1}{\gamma M_1^2} \left[1 - \sqrt{(\gamma + 1)\left(1 + \frac{\gamma - 1}{2}M_1^2 + \frac{\gamma + 1}{16}M_1^4\right)} \right] \qquad (3.9b)$$

As M_1 increases, δ_{max} increases as well so that if a wedge with a given turning angle accelerates from low to high Mach number, the shock can be detached at the low Mach numbers and become attached at the higher Mach number. [11]. Hence the front side of the wedge can be treated as normal shock wave. [12]
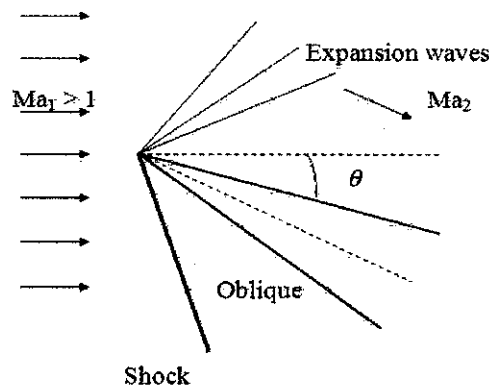
3.1.5   Prandtl-Meyer Waves Modelling

Figure 3.5: Prandtl-Meyer Wave.

Prandtl-Meyer expansion waves occur when the angle of attack becomes higher than the wedge deflection angle where the nature of flow is expanded. The change in properties occurs gradually across a series of waves emanating at the surface.

The turning angle:

$$\theta = v_2 - v_1 \qquad (3.10a)$$

where $v = f(M)$ as shown in the relation

$$v = \sqrt{\frac{\gamma + 1}{\gamma - 1}} \, tan^{-1} \sqrt{\frac{\gamma - 1}{\gamma + 1}(M^2 - 1)} - tan^{-1}\sqrt{M^2 - 1} \qquad (3.10b)$$

The change of properties across these waves is isentropic, so both the stagnation temperature, T_0 and stagnation pressure, P_0 are constants. Downstream Mach number M_2 can be found from equation (3.10b) by iteration (substituting v_2). The other flow properties downstream of the expansion can be calculated by using the isentropic flow relations.
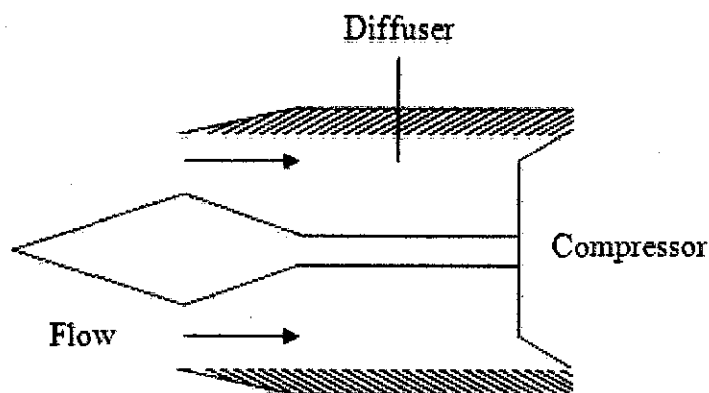
3.2   MODELLING OF DIFFUSER FLOW

Figure 3.6: Diffuser Part of the Intake.

Assumptions:

Steady, $\frac{\partial}{\partial t} = 0$

Viscous, $\mu \neq 0$

No body force, $\rho g = 0$

Compressible flow, so density not constant and can be evaluated by the equation of state:

$$\rho = \frac{P}{RT} \qquad (3.11)$$

The continuity equation

$$\left[\frac{\partial(\rho u)}{\partial x} + \frac{\partial(\rho v)}{\partial y}\right] = 0 \qquad (3.12a)$$

X-momentum:

$$\left(\rho u \frac{\partial u}{\partial x} + \rho v \frac{\partial u}{\partial y}\right) = -\frac{\partial p}{\partial x} + \mu\left(\frac{\partial^2 u}{\partial x^2} + \frac{\partial^2 u}{\partial y^2}\right) \qquad (3.12b)$$

Y-momentum:

$$\left(\rho u \frac{\partial v}{\partial x} + \rho v \frac{\partial v}{\partial y}\right) = -\frac{\partial p}{\partial y} + \mu\left(\frac{\partial^2 v}{\partial x^2} + \frac{\partial^2 v}{\partial y^2}\right) \qquad (3.12c)$$

Energy Equation

$$\frac{\partial\left(\rho\left(e + \frac{V^2}{2}\right)u\right)}{\partial x} + \frac{\partial\left(\rho\left(e + \frac{V^2}{2}\right)v\right)}{\partial y} = \frac{\partial}{\partial x}\left(k\frac{\partial T}{\partial x}\right) + \frac{\partial}{\partial y}\left(k\frac{\partial T}{\partial y}\right)$$

$$+ \frac{\partial}{\partial x}\left(-up + u\tau_{xx} + v\tau_{xy}\right) + \frac{\partial}{\partial y}\left(-vp + u\tau_{yx} + v\tau_{yy}\right) \qquad (3.12d)$$

3.3 TURBULENCE MODELLING

The flow turbulence in this study was simulated by using the standard k-epsilon model with enhanced wall treatment. In the k-epsilon model, two additional transport equations are being solved which are the turbulence kinetic energy, k and the turbulence dissipation rate, ε. The turbulence viscosity is then computed as a function of k and ε.

The turbulence kinetic energy, k, and its rate of dissipation, ε, are obtained from the following transport equations:

$$\frac{\partial}{\partial t}(\rho k) + \frac{\partial}{\partial x_i}(\rho k u_i) = \frac{\partial}{\partial x_j}\left[\left(\mu + \frac{\mu_t}{\sigma_k}\right)\frac{\partial k}{\partial x_j}\right] + G_k + G_b - \rho e - Y_M + S_k \quad (3.13)$$

And

$$\frac{\partial}{\partial t}(\rho \epsilon) + \frac{\partial}{\partial x_i}(\rho \epsilon u_i)$$
$$= \frac{\partial}{\partial x_j}\left[\left(\mu + \frac{\mu_t}{\sigma_\epsilon}\right)\frac{\partial \epsilon}{\partial x_j}\right] + C_{1\epsilon}\frac{\epsilon}{k}(G_k + C_{3\epsilon}G_b) - C_{2\epsilon}\rho\frac{\epsilon^2}{k} + S_\epsilon \quad (3.14)$$

Where

G_k = generation of turbulence kinetic energy due to mean velocity
     gradients

G_b = generation of turbulence kinetic energy due to buoyancy

Y_M = contribution of the fluctuating dilatation in compressible turbulence
     to the overall dissipation rate

The turbulent viscosity, μ_t is computed by combining k and ε as follows:

$$\mu_t = \rho C_\mu \frac{k^2}{\varepsilon} \quad (3.15)$$

where $C\mu$ is a constant.

20

For the model constants $C_{1\varepsilon}$, $C_{2\varepsilon}$, C_μ, σ_k and σ_ε, the default values set by FLUENT are being used. The values used are as follows:

$C_{1\varepsilon}$ = 1.44

$C_{2\varepsilon}$ = 1.92

C_μ = 0.09

σ_k = 1.0

σ_ε = 1.3

These values are being used in this study because the default values have been determined experimentally and have been found to work fairly well for wide range of wall-bounded and free shear flows.

CHAPTER 4

METHODOLOGY

Some previous researchers have simulate the entire flow field of the spiked intakes, e.g. Stater et al(2002).In present work, the field will be divided into two parts, the external part and the internal part.

4.1   TECHNIQUE OF ANALYSIS

The analysis will be conducted by simulating the flow field:

a. The external part (the shock wave system), to be modelled and analyzed analytically. The shock wave system is modelled by using programming in Microsoft Excel.

b. The internal part (the diffuser), to be simulated and analysed numerically using CFD software.

c. Simulation and analysis will be done at different angle of attack and Mach number. The results are then to be verified by comparing with another previous work done.

4.2 WORK FLOW CHART

The planned work flow for the project is as shown below.
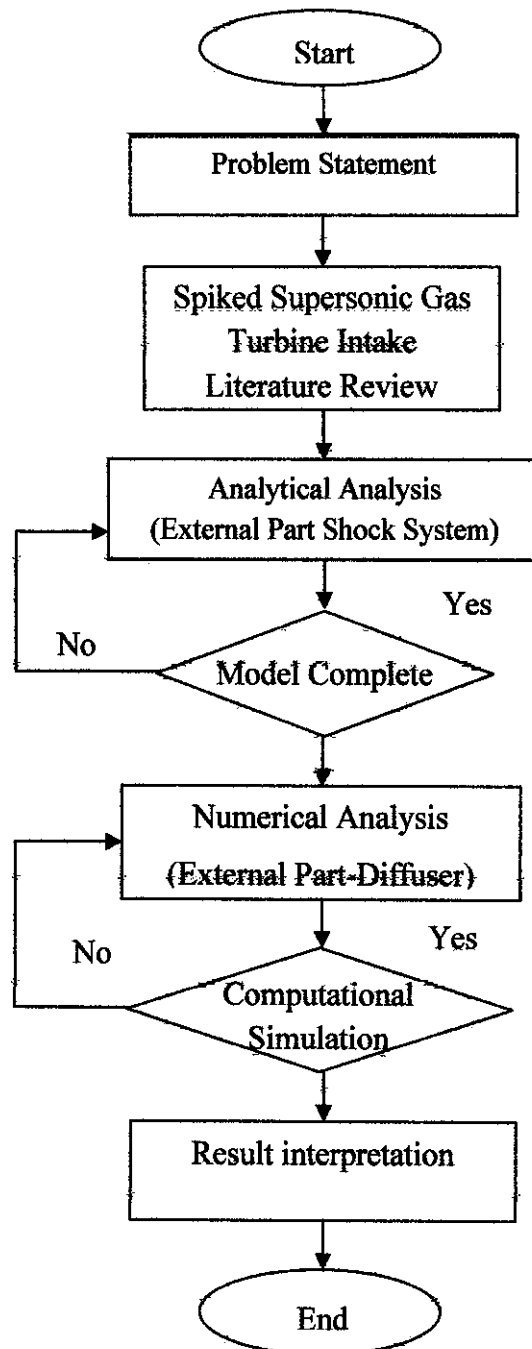
Figure 4.1: Flow chart of the project.

4.3   GANTT CHART

No	Detail/ Week	1	2	3	4	5	6	7	8	9	10	MID SEMESTER BREAK	11	12	13	14
1	Selection of Project Topic	■	■													
2	Preliminary Research Work • Research on spiked supersonic gas turbine intake		■	■	■	■	■	■	■							
3	Submission of Preliminary Report				●											
4	Analysis and modelling of the shock wave system					■	■	■	■	■	■		■			
5	Submission of progress Report								●							
6	CFD simulation attempt • Attempt to draw the geometry and meshing technique										■		■	■	■	
7	Submission of Interim Report Final Draft														●	
8	Oral Presentation															●

No	Detail/ Week	1	2	3	4	5	6	7	8	9	10		11	12	13	14
1	Computational Simulation	■	■	■	■	■	■									
2	Submission of Progress Report 1				●											
3	Results Interpretation • Study the Results from FLUENT						■	■	■	■						
4	Submission of Progress Report 2 and Seminar								●							
5	Results Comparison									■	■		■			
6	Poster Exhibition										●					
7	Submission of Dissertation (Soft Bound)											M I D S E M E S T E R B R E A K		●		
8	Oral Presentation														●	
9	Submission of Project Dissertation(Hard Bound)															●

●   Suggested milestone

■   Process

Figure 4.2: Suggested milestone for the first and second half of Final Year Project

CHAPTER 5

ANALYTICAL ANALYSIS

This chapter consists of three sections, which are:

- The analytical analysis done using Microsoft Excel.
- The workflow of the program.
- The results from analytical solution

5.1 ANALYTICAL ANALYSIS

The external part (the shock system) of the diffuser is to be modelled and analysed analytically to solve the waves system in the upper part and the lower part of the diffuser. The output from the analytical analysis is then used as the input for the numerical analysis by using CFD software (FLUENT and GAMBIT).

In order to solve the external flow, a program is created using Microsoft Excel. The program basically consists of three main parts which is called program OSW (oblique shock relation), program NSW (normal shock relation) and program P-M (Prandlt-Meyer shock relation)

The required information to be inputted into the program is M, α, δ, γ, H which vary in the range, as below:

M_∞	:	1.4 - 3.0
α	:	0°-10°
δ	:	6°
H	:	10 000m
γ	:	1.4

5.1.1 Program OSW

This program calculates the flow properties just after the oblique shock wave from Eqn. (3.7).

Input   : M_1, P_1, ρ_1, T_1, P_{o1}, γ, δ, ν_1

Output   : M_2, P_2, ρ_2, T_2, V_2, P_{o2}, σ

5.1.2 Program NSW

This program calculates the flow properties behind the normal shock wave from Eqn. (3.8).

Input   : M_x, P_x, ρ_x, T_x, P_{ox}, γ

Output   : M_y, P_y, ρ_y, T_y, V_y, P_{oy}

5.1.3 Program P-M

This program calculates the flow properties behind the Prandtl-Meyer waves from Eqn(3.10).

Input: M_1, P_1, ρ_1, T_1, P_{o1}, γ, R, δ, ν_1

Output: ν_2, M_2, P_2, ρ_2, T_2, V_2, P_{o2}

5.1.4 REFLECT

This program calculates the flow properties behind the reflected O.S.W inside the intake, from Eqn(3.7) and Eqn(3.8).

The results of the program have been verified by comparing with the standard gas tables.

27

5.2 WORK FLOW OF ANALYTICAL ANALYSIS

Leeside   Windward side

$\delta = \delta_z - \alpha$ $\delta = \delta_z + u$

$\delta_z < \delta_{Max}$ NO $\delta_z < \delta_{Max}$

YES

OSW   NSW   OSW

$\delta_z = 0$ $\delta_z = 0$

NO   NO

OSW   YES   OSW   YES

$M < 1$ YES $M < 1$ YES

NO

$\sigma < \theta$ $\sigma < \theta$

YES   NO   YES   NO

REFLECT   NSW   REFLECT   NSW

NSW   NSW

END

C

Leeside   Windward side

$\delta = 0$ $\delta = \delta_z + u$

NO $\delta_z < \delta_{Max}$

YES

NSW   OSW

$\delta_z = 0$ $\delta_z = 0$

NO   NO

OSW   YES   OSW   YES

$M < 1$ YES $M < 1$ YES

NO   NO

$\sigma < \theta$ $\sigma < \theta$

YES   NO   YES   NO

REFLECT   NSW   REFLECT   NSW

NSW   NSW

END
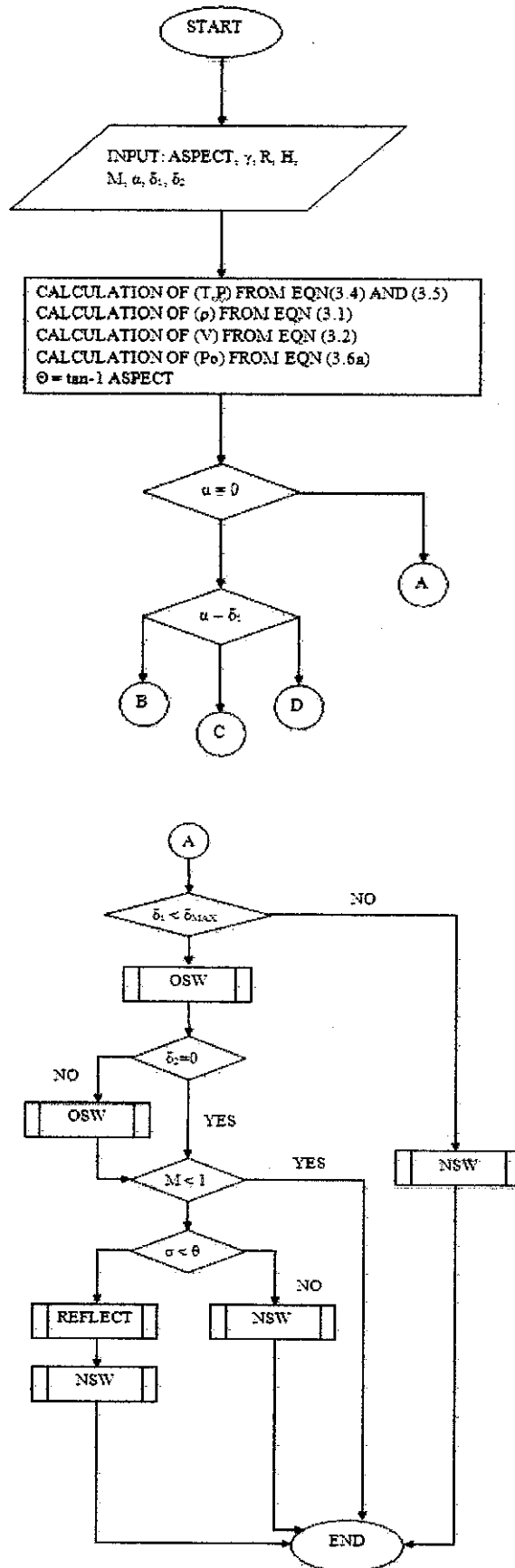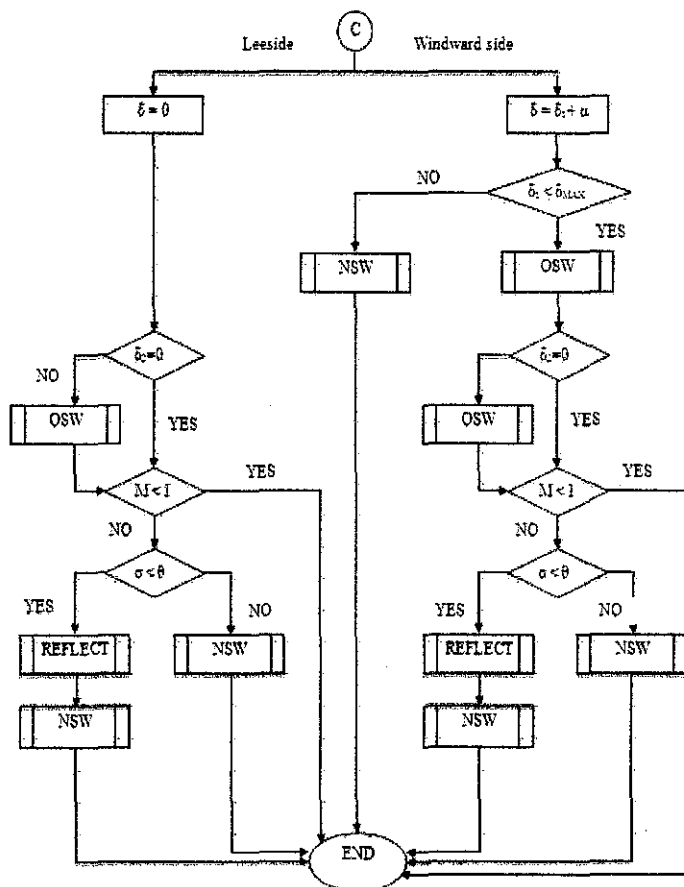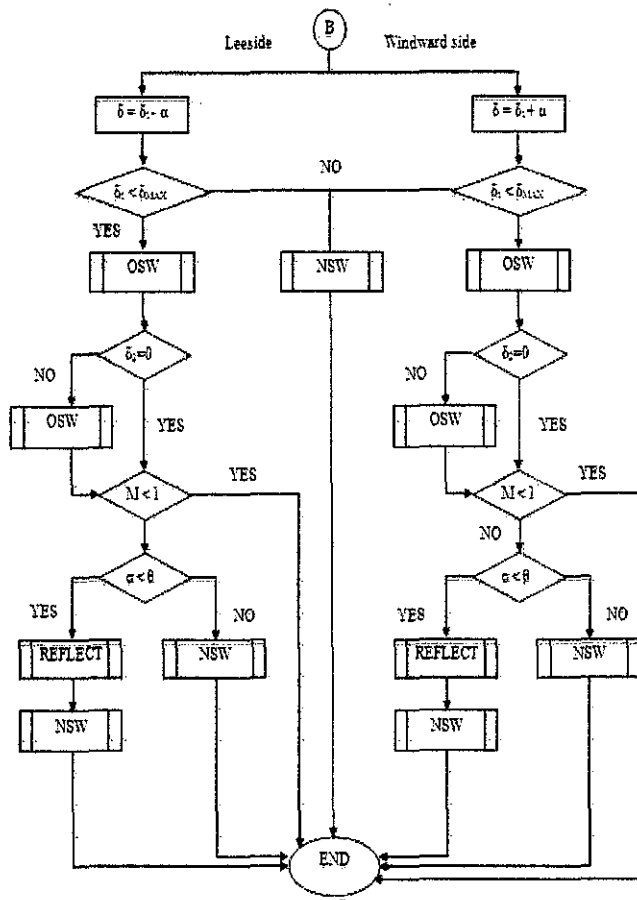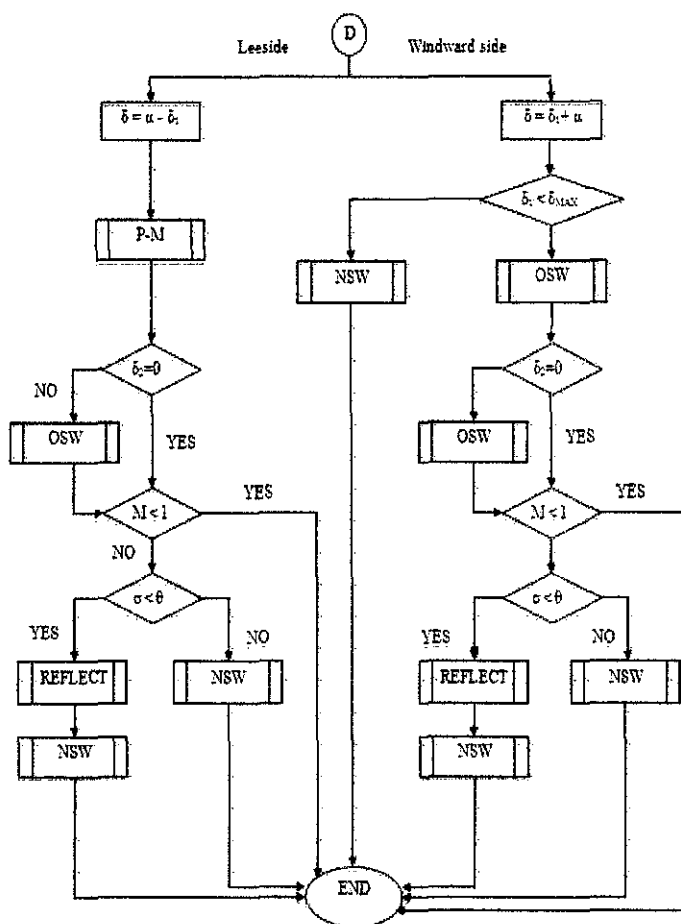
Figure 5.1: Flow chart of the program for analytical solution.

5.3 VERIFICATION OF PROGRAM FOR ANALYTICAL ANALYSIS

After the completion of the program OSW, program NSW and program P-M, the results from this program are being compared with oblique shock properties graph, normal shock properties graph and Prandtl-Meyer properties table respectively. The results as shown in Table 5.1, 5.2 and 5.3 show that the programs agreed with the value from the standard properties graph and table. Hence, these programs can be used for the analytical analysis.

Table 5.1: Results comparison for program OSW

M_a	Shock Wave Angle (degrees)	
	Program OSW	O.S Properties Graph
1.8	39.48	39.5
2.0	35.24	35

Table 5.2: Results comparison for program NSW

	$Ma_x = 1.8$		$Ma_x = 2.0$	
	Program NSW	N. S. Properties Table	Program NSW	N. S. Properties Table
M_y	0.6165	0.6165	0.5774	0.5774
P_y/P_x	3.613	3.613	4.5	4.5
ρ_y/ρ_x	2.359	2.359	2.667	2.667
T_y/T_x	1.532	1.532	1.687	1.687
P_{oy}/P_{ox}	0.8127	0.8127	0.7209	0.7209

Table 5.3: Results comparison for program P-M

M_1	M_2	
	Program P-M	P-M Properties Table
1.5	2.208	2.208
2.0	2.831	2.831

CHAPTER 6

RESULTS AND DISCUSSION

This chapter consists of three sections, which are:

- Modelling of diffuser.
- Results from the numerical analysis.

6.1 MODELING OF DIFFUSER

The same geometry used by *Abbood A.H [13]* is being adopted in the numerical analysis. The diffuser is modelled by using GAMBIT. The geometry and the vertices of the diffuser are shown in Figure 6.1. For the sake of FLUENT, an extension of about 50% of the diffuser length of the numerical domain is necessary to prevent the occurrence of excessive reversed flow at the outlet [17]

For the boundary types, the inlet of the diffuser is set to be 'MASS FLOW INLET'; outlet is set to be 'PRESSURE OUTLET'; upper and lower wall is set to be 'WALL'.

(1.0, 0.5)

(0, 0.329)

(0, 0)

(1.0, 0)
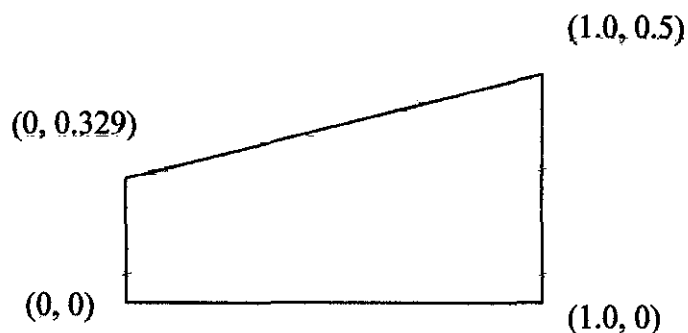
X & y axes not to Scale, All Dimensions in Metres (m).

Figure 6.1: Diffuser geometry with vertices.
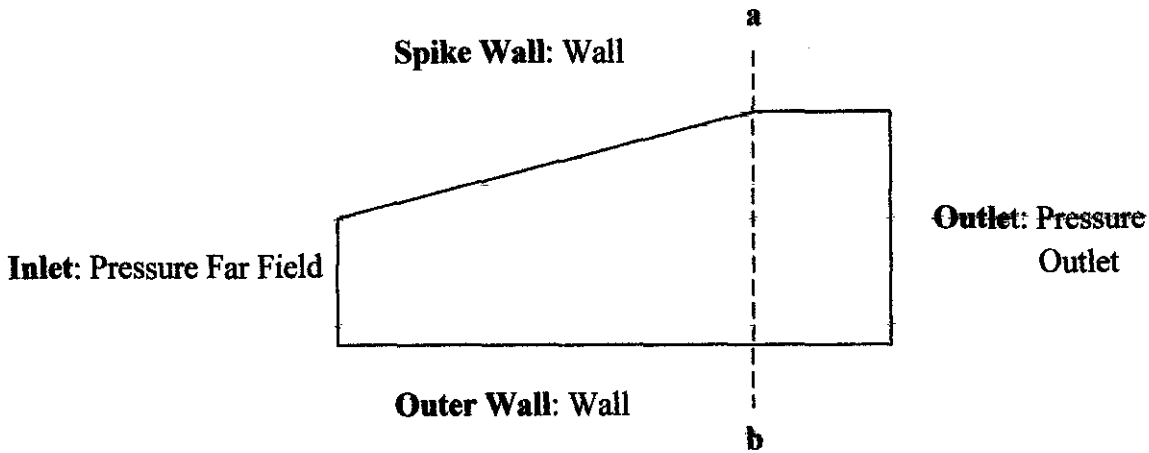
Figure 6.2: Boundary types of the diffuser.

6.1.1 Computational Grid Generation

The grid for the diffuser is generated by using GAMBIT as well. In order to establish the adequacy of the finite element mesh required to obtain an accurate results, three different meshes are generated. Mesh M1 consists of 40*120 grids by using quadrilateral cells. For mesh M2 and M3 the meshes used are 50*150 grids and 60*180 grids respectively. The three different meshes are tested under the same input parameters in FLUENT which is at Ma= 1.8, δ=6.0 and α=0. The solutions obtained with the three meshes are shown in Figure. From the results obtained, mesh M1 and mesh M2 results are quite similar in terms of pressure recovery and percentage error. As for the mesh M3, the results are the closest to the results from Ref [5] but it required a lot more computational time compared to mesh M1 and M2. Since mesh M1 and M2 results are quite similar, this suggests that mesh M1 is adequate to accurately capture all the details associated with the flow with minimal computational time. Hence, all the remaining part of the study will be computed by using mesh M1.
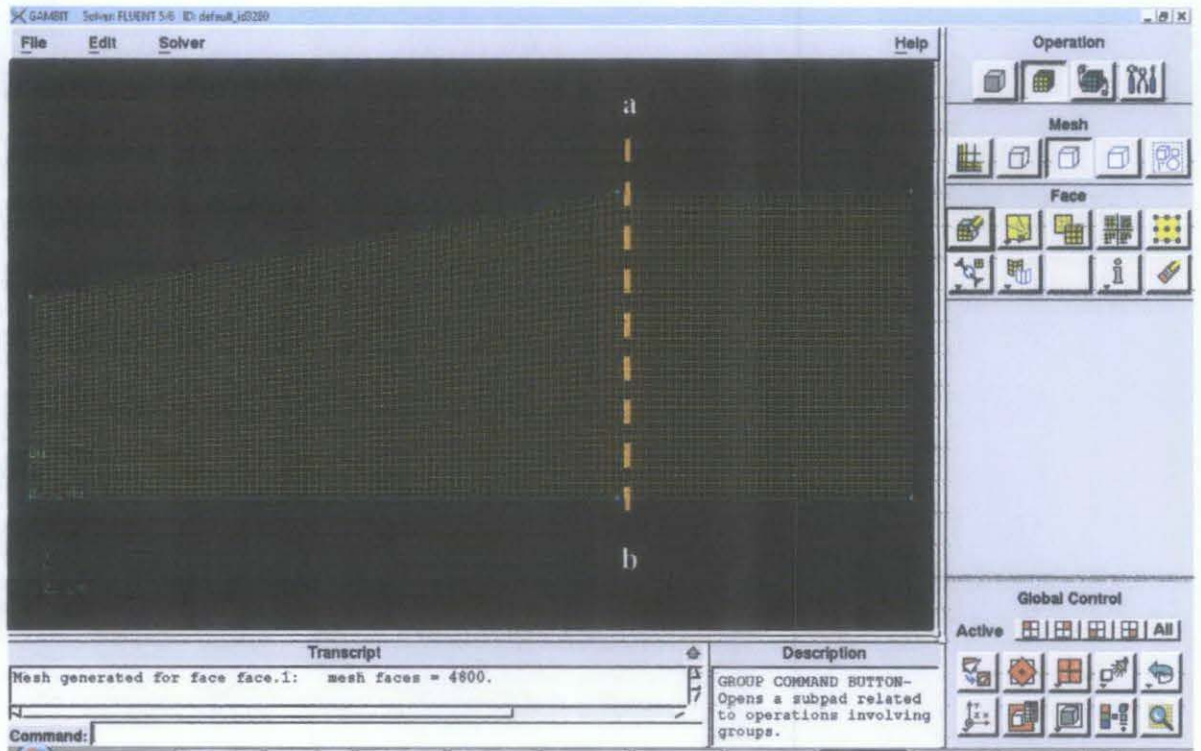
Figure 6.3: Diffuser inlet grid (40 × 120 quadrilateral cells).

Note: a-b is the line of interest for the numerical analysis.

Table 6.1: Pressure recovery for different mesh sizes

Mesh Name	Mesh Size	P_e(kPa)	$Pe/P_{o\infty}$	Ref($Pe/Po\infty$)	% Error
M1	40*120	109.734	0.7207	0.745	3.26
M2	50*150	109.709	0.7205	0.745	3.29
M3	60*180	109.924	0.7219	0.745	3.1

6.2 RESULTS FROM NUMERICAL ANALYSIS

6.2.1 Results Comparison with Previous Numerical Work

A comparison has been done between the results from the CFD work of this study with the previous numerical work [5]. This comparison is done to verify the accuracy of the model done using the commercial CFD software.

In this comparison, the effect of angle of attack on the pressure recovery at the leeside and windward side is being used. The comparison is done with Ma=1.8 at constant wedge angle which is at 6°. The graphs for leeside and windward side are being plotted as shown in Figure 6.4 and Figure 6.5. From the comparison done, the percentage difference between the current work and previous numerical work [5] is less than 9% deviation. Since the percentage difference is less than 10%, the results are verified to be accurate. The main reason of this difference in results is because in the current work the turbulence modelling is taken into consideration while the previous work did involve it in the analysis.
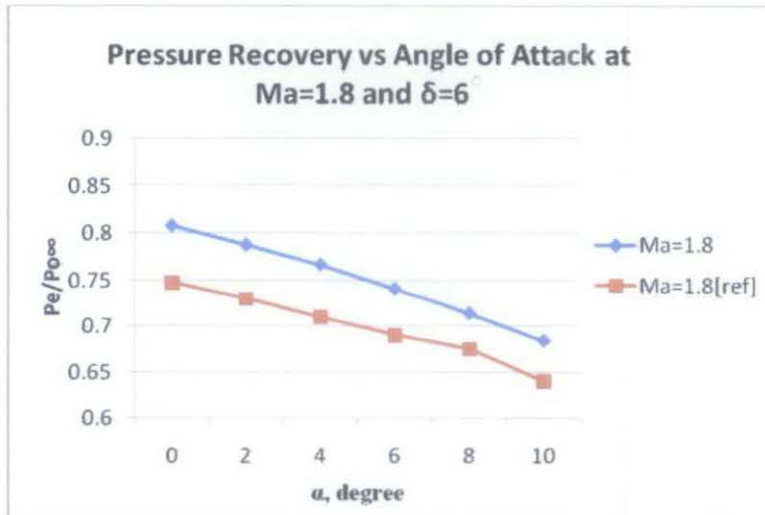
Figure 6.4: Results comparison at leeside for Ma=1.8.
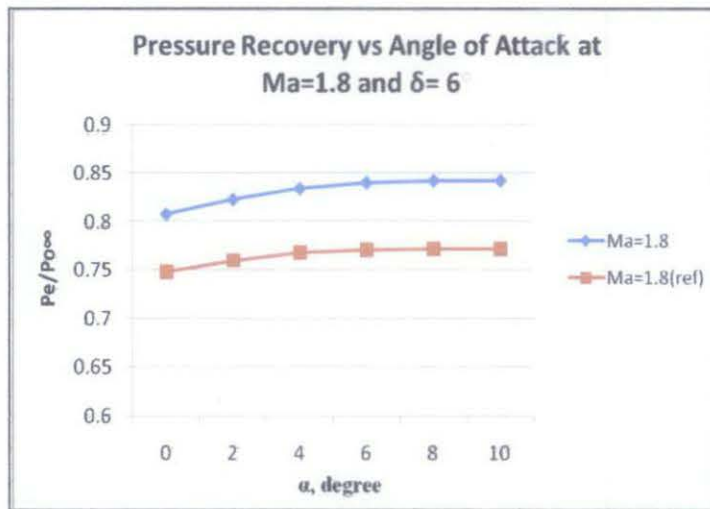
Figure 6.5: Results comparison at windward side for Ma=1.8.

6.2.2 Effect of Angle of Attack and Mach number

This study illustrates the effect of changing the angle of attack at different Mach no on the pressure recovery at constant wedge angle.

Figure 6.6 indicates that in the leeside of the spike, the pressure recovery decreases by increasing the angle of attack for all the Mach number. This phenomenon shows that there is a loss in body compression, because by increasing the angle of attack in the leeside it reduces the effective deflection angle.

Figure 6.7 indicates that in the windward side of the spike, the pressure recovery increases by increasing the angle of attack. The reason is because the increase in angle of attack in the windward side increases the effective deflection angle, hence leading to a stronger shock. Considering Ma=1.4, as the angle of attack increases from $2°$, the pressure recovery decreases and becomes constant. At low Mach number, the deflection angle increases and exceeded the maximum deflection angle. This will eventually cause the occurrence of detached shock waves.

It can be observed as well that the pressure recovery decreases as Mach no increases because as Mach no increases the shock angles will decrease and become very weak. The decrease of shock angle will cause the shock reflects inside the intake, resulting to decrease of pressure recovery.

36
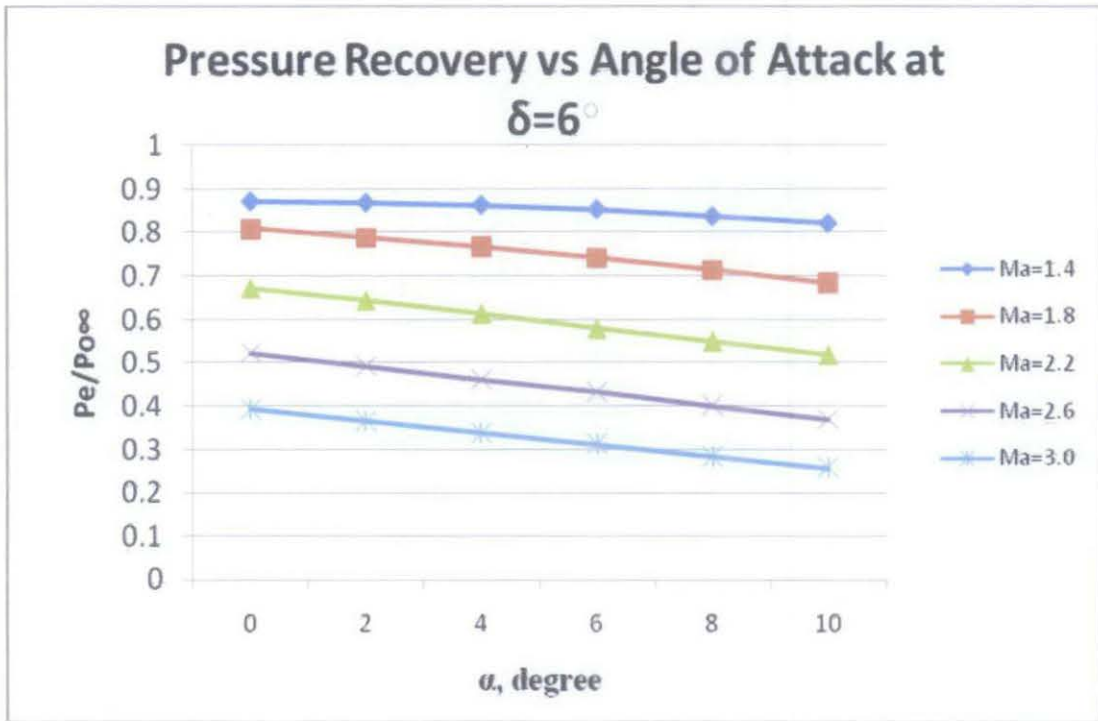
Figure 6.6: The effect of angle of attack on the pressure recovery at leeside.
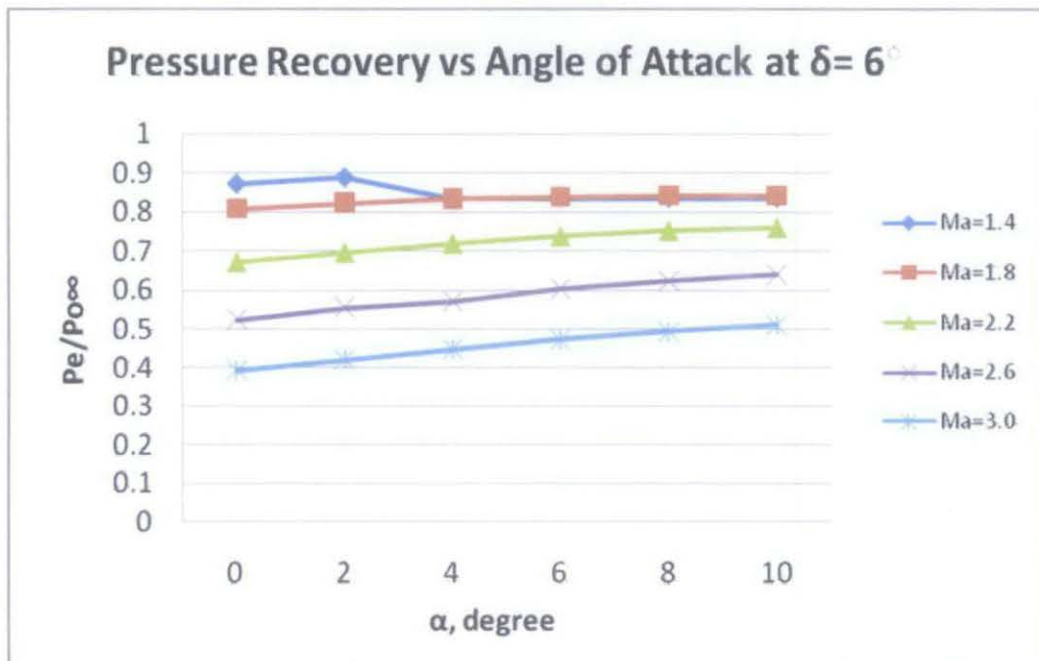
Figure 6.7: The effect of angle of attack on the pressure recovery at windward side.

6.2.3 Static Pressure Contour

The contour of static pressure for both sides of the diffuser is being created by using FLUENT software. The contour shown are done at Ma=2.2 with different angle of attacks(δ=0, δ=4, δ=10).

From Figure 6.8 it can be observed that the contour at the leeside and windward side are identical, because the analysis is done at zero angle of attack. At zero angle of attack, the deflection angle at created by the spike is identical at both sides of the spike. Hence, the pressrue distribution at the leeside and windward side of the diffuser will also be identical.

In Figure 6.9 and Figure 6.10, they represent the static pressure contour at δ=4 and δ=10 respectively. At δ=4 and δ=10, the deflection angle at the leeside and windward side of the spike will be different. These difference in deflection angle will eventually cause the pressure distribution at the leeside and windward side of the diffuser to be different. At a higher angle of attack(δ=10) shown in Figure 6.10, the difference in pressure distribution will be more significant compared to lower angle of attack(δ=4) as shown in Figure 6.9.
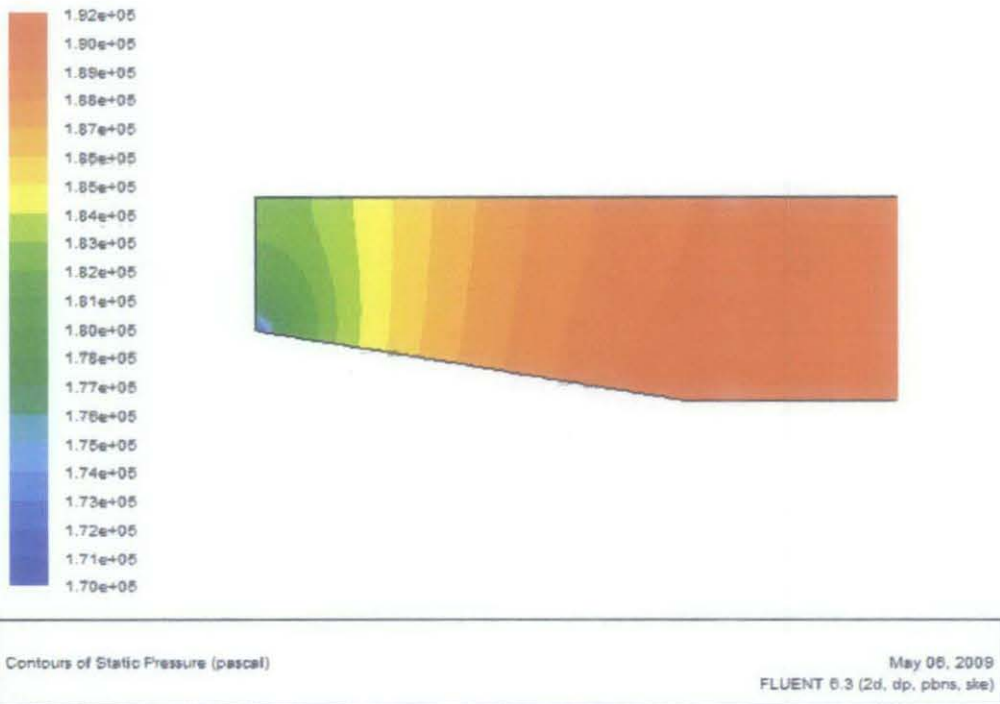
(a)
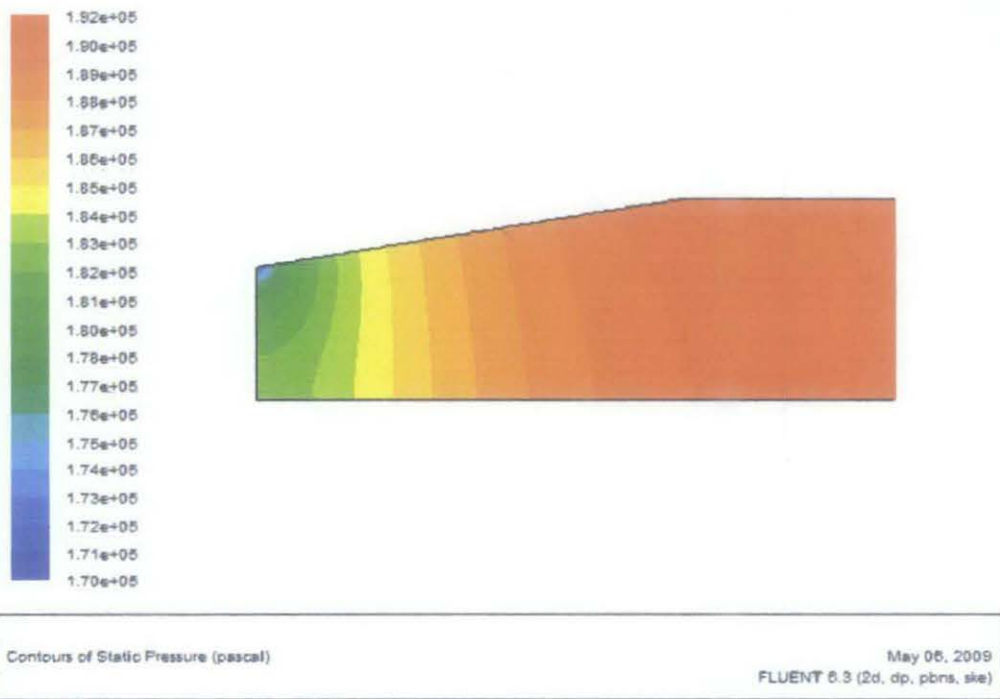
(b)

Figure 6.8: Contour of static pressure for leeside and windward side at Ma=2.2, δ=0.
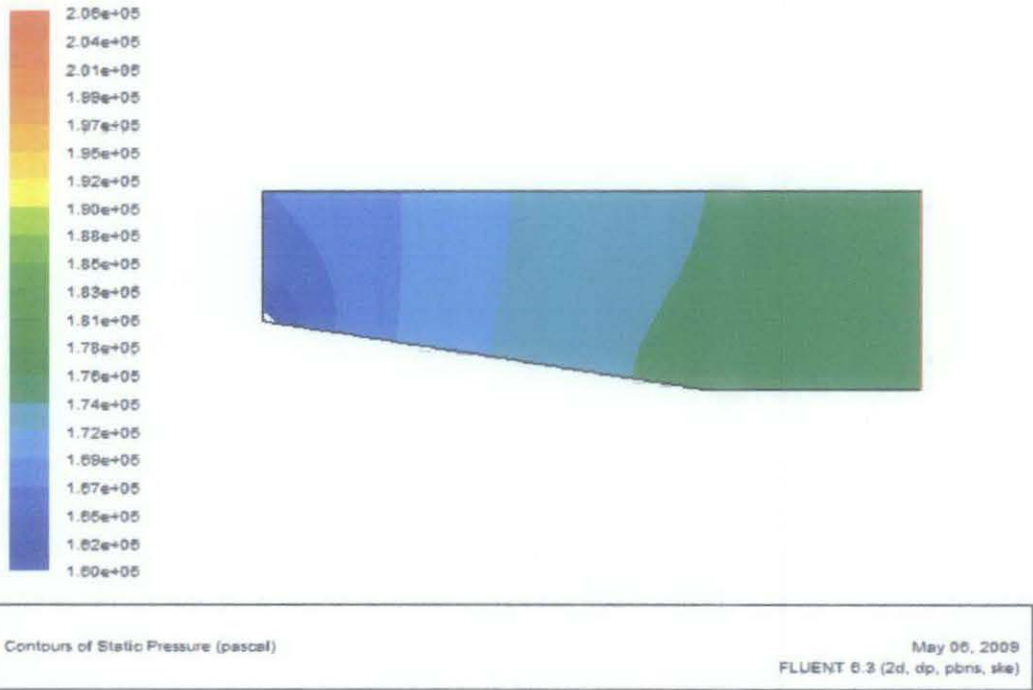
(a)

(b)

Figure 6.9: Contour of static pressure for leeside and windward side at Ma=2.2, δ=4.

Contours of Static Pressure (pascal)

May 06, 2009
FLUENT 6.3 (2d, dp, pbns, ske)

(a)

Contours of Static Pressure (pascal)

May 06, 2009
FLUENT 6.3 (2d, dp, pbns, ske)
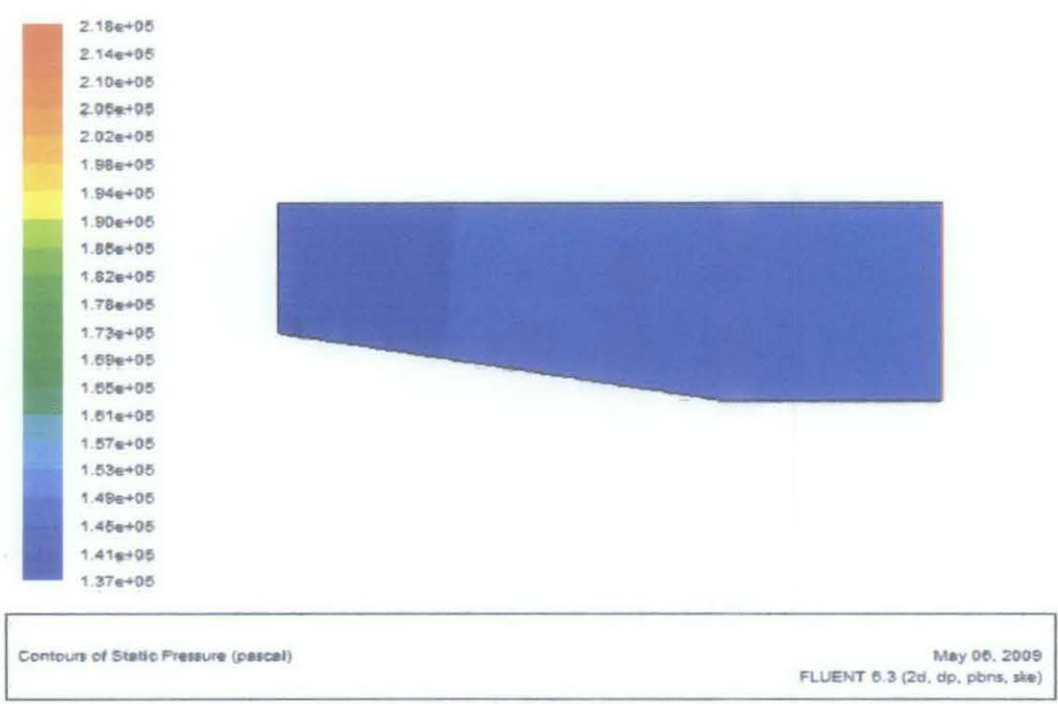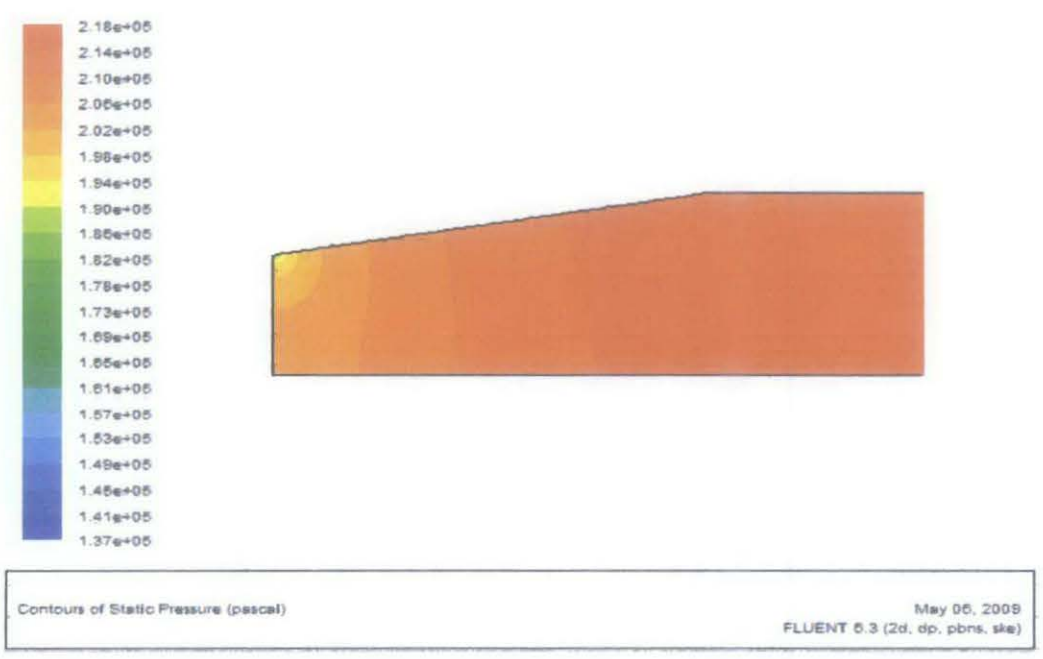
(b)

Figure 6.10: Contour of static pressure for leeside and windward side at Ma=2.2, δ=10.

6.2.4 Contour of Static Temperature

Figure 6.11 shows the temperature contour for leeside and windward side at zero angle of attack. As the flow moving towards the compressor face (x-direction), the temperature increases. Due to zero angle of attack the temperature distribution at both sides are identical. In addition the temperature contour indicates that at the region near the spiked wall, the temperature is higher in comparison with the outside wall region. This is because at the spike wall region, the flow slows down faster (Figure 6.12) than the region in the outside wall. Hence, from the energy equation this will cause the rise in temperature at the spike wall region
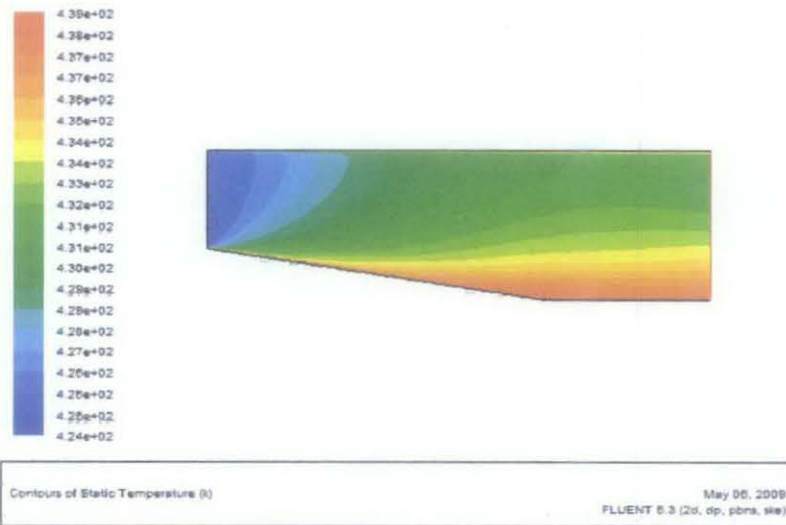
(a)
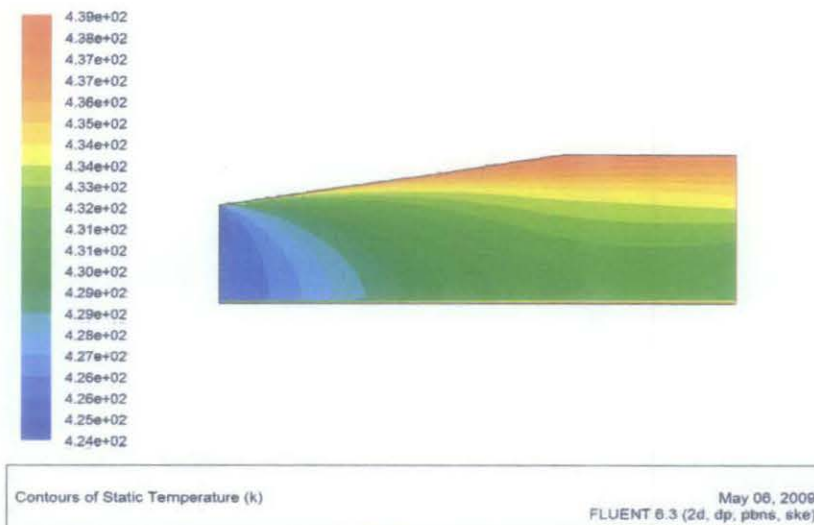
Figure 6.11: Contour of static temperature for leeside and windward side at Ma=2.2, $\delta=0°$.

As shown in Figure 6.12, when it is at $10°$ angle of attack, the temperature distribution will be higher at the leeside in comparison with the windward side.
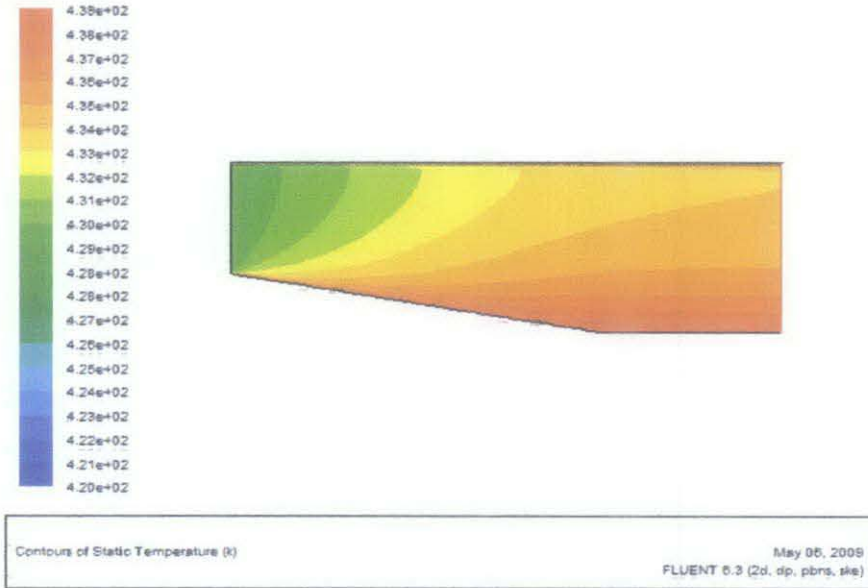
(a)
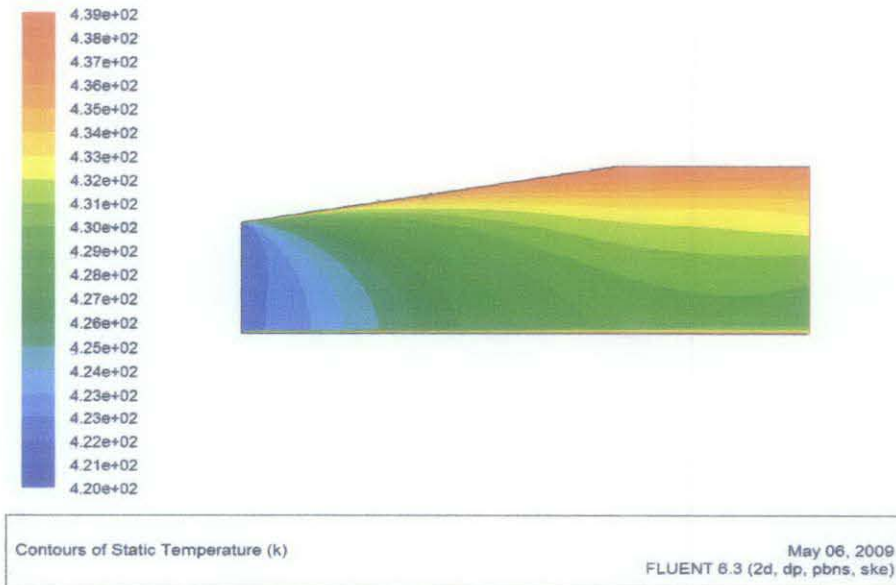
(b)

Figure 6.12: Contour of static temperature for leeside and windward side at Ma=2.2, $\delta=10°$.

6.2.5 Contours of Velocity Magnitude

Figure 6.13 shows the velocity distribution at the leeside and the windward side at zero angle of attack. At the region close to the wall, the velocity is indicated by blue region indication zero velocity. This shows the fluid flowing over a stationary surface comes to a complete stop at the surface due to the non-slip condition.
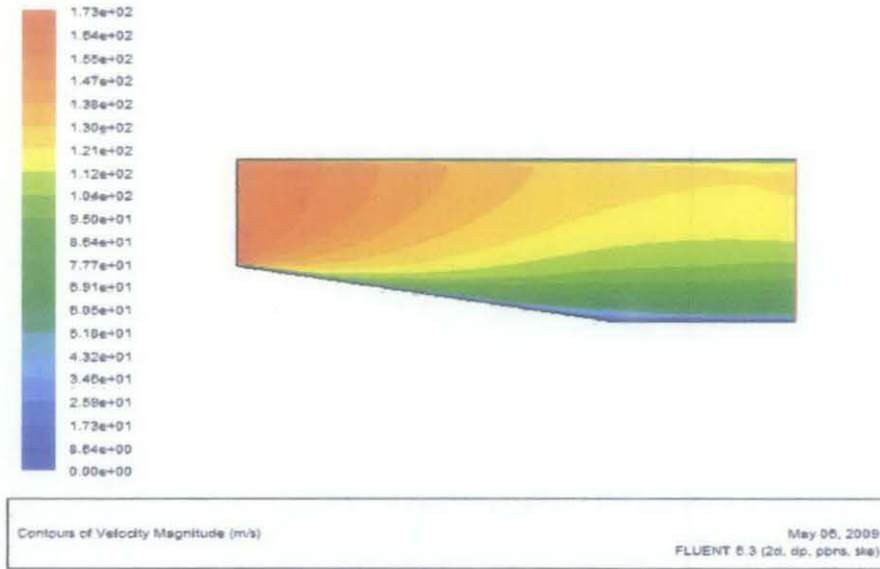
(a)
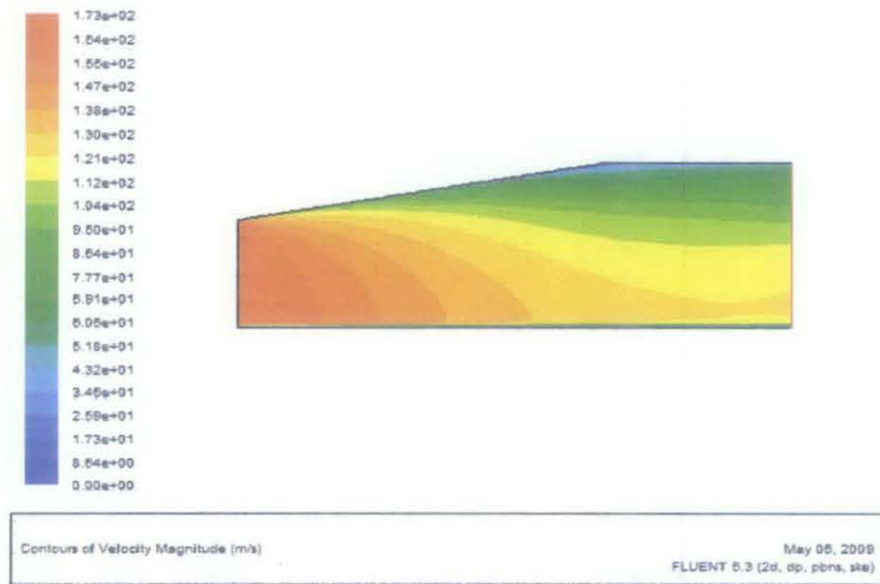
(b)

Figure 6.13: Contour of velocity for leeside and windward side at Ma=2.2, δ= $0°$.
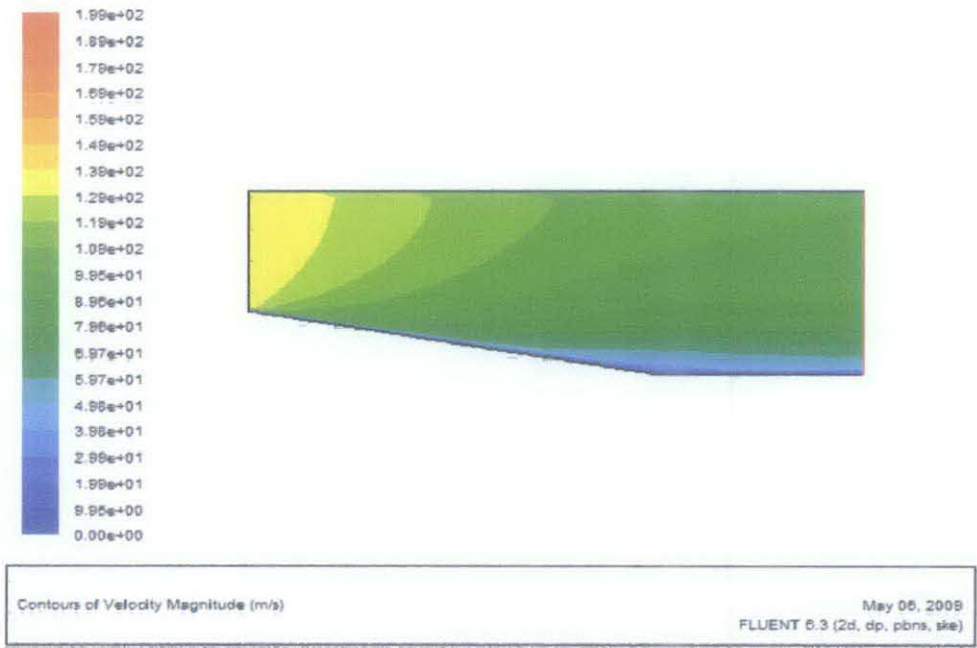
(a)
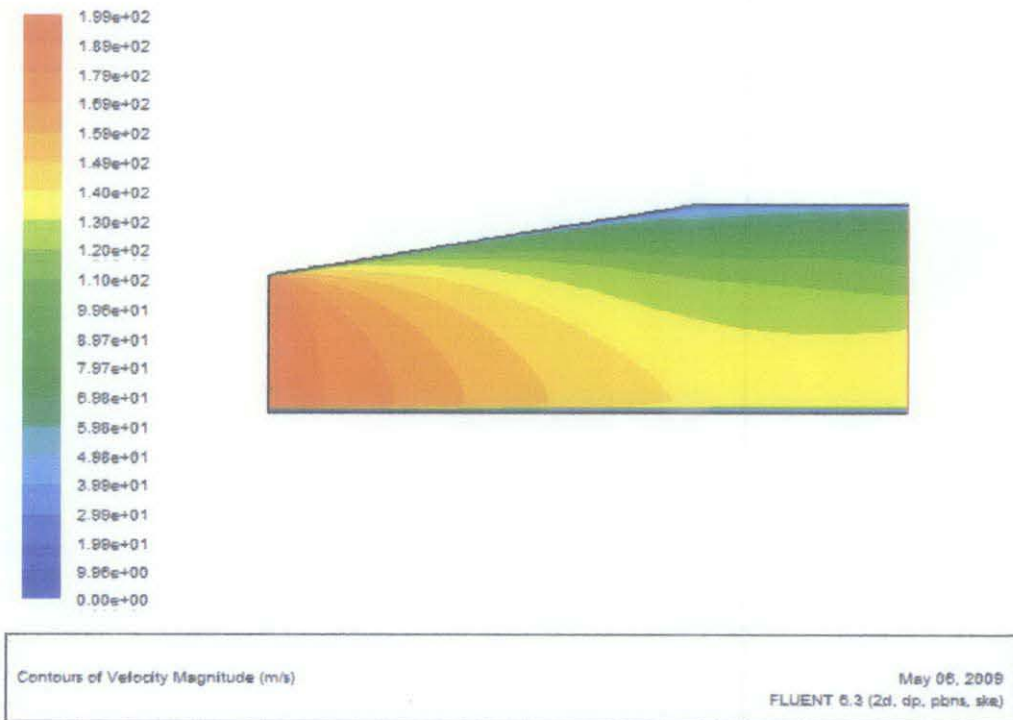
(b)

Figure 6.14: Contour of velocity magnitude for leeside and windward side at Ma=2.2, δ=10.

CHAPTER 7

CONCLUSION

The analysis of the flow in the supersonic intake is modelled by dividing the flow field into two regions. The outer part which consists of the waves system is modelled and analysed analytically. On the other hand, the internal part of the diffuser is modelled and analysed numerically using Fluent and Gambit.

6.1 CONCLUSIONS

From the numerical analysis, it shows that the pressure recovery degrades at the leeside with the increase of the angle of attack. On the other hand, the pressure recovery increases at windward side of the intake by increasing the angle of attack. By increasing the Mach number, the pressure recovery will decrease at both leeside and windward side.

The numerical simulation was performed successfully. The results obtained for the numerical analysis of the present work are in agreement with those obtained numerically by previous investigation. The simulation has been proven to be able to characterize the supersonic intake and the pressure recovery at the face of the compressor is predicted with good accuracy. The simulation also is able to characterize the temperature and velocity distribution in the diffuser. In addition, it is very important to include the turbulent effect into the modelling to acquire a more accurate result.

The incidence angles and Mach number hold a significant effect on the flow structure which affected the pressure distribution in the diffuser part of the gas turbine intake.

46

Therefore, it is very essential to simulate numerically the spike intake as it will be able to predict the flow characteristic more accurately.

6.2 RECOMMENDATIONS FOR FUTURE WORKS

With the completion of the present work, it can be extended further by adding more complicated aspects to achieve a more complete analysis of the spike supersonic gas turbine inlet.

There are a few suggestions that could be the topic of research for the future work within the same field:-

1. Perform simulation on a double wedge spike. i.e. 'A three shock intake'. Simulation on the double wedge spike is a much complex analysis. At zero angle of attack, the flow will go through two oblique shock waves at different shock angles before flowing through the normal shock waves. Theoretically this might improve the pressure recovery in the diffuser. Hence the analysis involving double wedge worth being investigated.
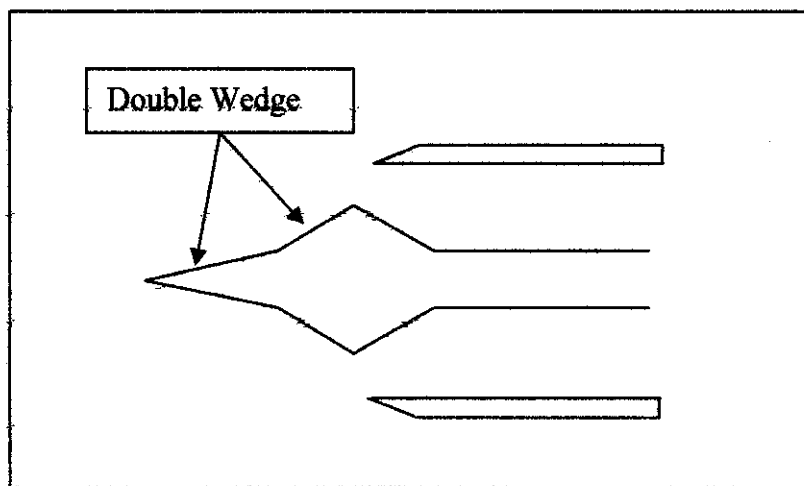
2. Changing the geometry of the spike to two-dimensional gradual isentropic compression, i.e., curved surface spike.

REFERENCES

[1] Klause Hunecke (1997), "Jet Engines: Fundamentals of Theory Design And Operation", Airlife Publishing Ltd

[2] J. Seddon, E.L. Goldsmith(1993), "Practical Intake Aerodynamic Design", Blackwell Scientific Publications.

[3] Al-Kayiem.H.H and T.Wesmi M.Salih (2003), "The Effect of Incidence and Forebody Angles on the Performance of Spiked Supersonic Intake"

[4] Al-Kayiem.H.H and Aboud A.S (2007), 'Flow Analysis in Spiked Supersonic Intakes of A/C (I-Inviscid)', Conference of Aerospace Technology of XXI Century.

[5] T.Wesmi M.Salih (2002), 'The Flow Analysis of the Spiked Supersonic Intake', MSc.Thesis, the college of Engineering Al-Mustansiris University.

[6] D.Beastall (1956), 'Flow Instability of Centre-body Diffusers at Supersonic Speeds', Aeronautical Research Council Reports and Memoranda.

[7] S.S.Gokhale and V.R.Kumar (2001), 'Numerical Simulation of Supersonic Inlet Flow', International Journal for Numerical Methods in Fluids.

[8] G.Raja Singh Thangadurai, B.S Subhash Chandra, V.Babu and T.Sundararajan (2004), 'Numerical Investigation of the Intake Flow Characteristics for a Ramjet Engine with and without Heat Addition in the Combustion Chamber', Defense Science Journal, Defense Science Journal, Vol.54, No.1, pp.3-16.

[9] M.K Jain & S.Mittal (2005), 'Euler Flow in a Supersonic Mixed-Compression Inlet', International Journal for Numerical Methods in Fluids.

[10] M.R.Soltani, M.Farahani and J.S. Younsi (2008), 'Performance Improvement of a Supersonic External Compression Inlet by Heat Source Addition', Proceeding of World Academy of Science, Engineering and Technology Volume 30.

[11] Patrik H. Oosthuizen and William E.Carscallen (1997), 'Compressible Fluid Flow', McGraw-Hill Company.

[12] Michel A.Saad (1985), 'Compressible Fluid Flow', Prentice-Hall INC.

[13] Abbood A.H.(1999), 'Numerical Analysis of Two-Dimensional Convergent-Divergent Nozzle for A Modern Fighter". MSc. Thesis, the college of Military Engineering.

[14] Yunus A. Cengel and John M.Cimbala (2006), 'Fluid Mechanics', McGraw-Hill company.

[15] National Aeronautics and Space Administration web site.
http://www.grc.nasa.gov/WWW/K-12/airplane/normal.html

[16] National Aeronautics and Space Administration web site.
http://www.grc.nasa.gov/WWW/K-12/airplane/oblique.html

[17] F.Depypere, J.G.Pieters and K.Dewettinck (2004), 'CFD Analysis of Air Distribution in Fluidised Bed Equipment', Food Technology and Engineering, Ghent University, Belgium.

APPENDICES

APPENDIX A: RUNNING FLUENT

1.   Launch FLUENT

Lab Apps > FLUENT 6.3.26

Select 2ddp (2D, double-precision version) from the list of options and click Run

2.   Import File

Main Menu > File > Read > Case...

3.   Analyze Grid

Main Menu > Grid > Check

Grid > Info > Size

Determine how many cells and nodes does the grid have.

Display > Grid

```
FLUENT [2d, dp, segregated, ske]
File  Grid  Define  Solve  Adapt  Surface  Display  Plot  Report  Parallel  Help

   Checking face handedness.
   Checking element type consistency.
   Checking boundary types:
   Checking face pairs.
   Checking periodic boundaries.
   Checking node count.
   Checking nosolve cell count.
   Checking nosolve face count.
   Checking face children.
   Checking cell children.
   Checking storage.
Done.

Grid Size

Level    Cells    Faces    Nodes    Partitions
   0     4800     9760     4961             1

1 cell zone, 5 face zones.
```
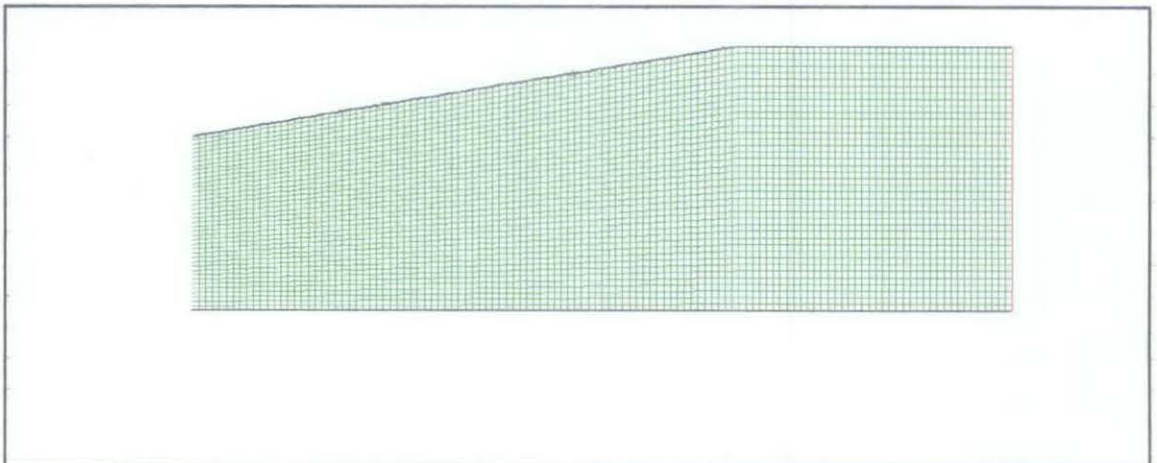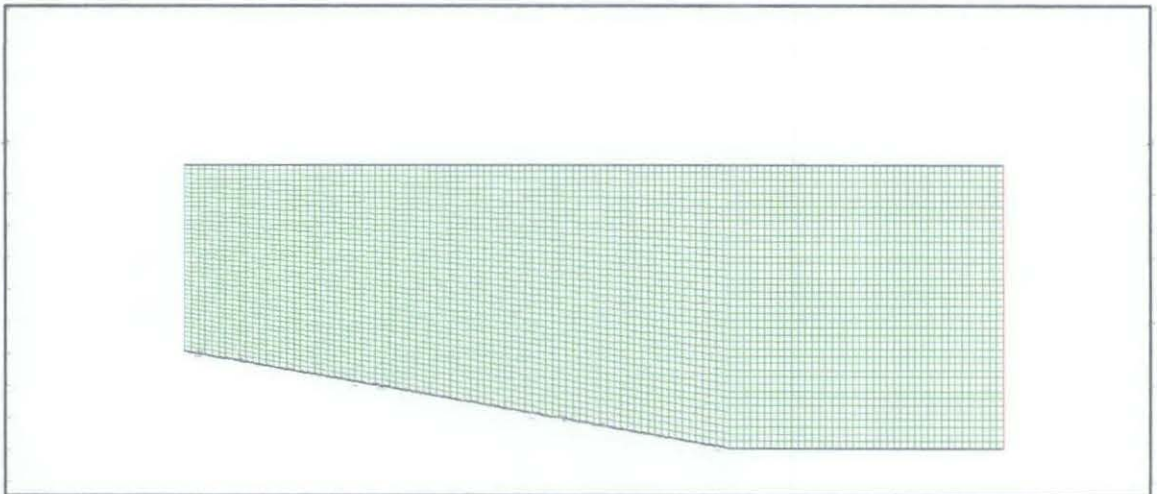

Any errors in the grid would be reported at this time. Check the output and make sure that there are no errors reported.

4. Define Properties

Define > Models > Solver...
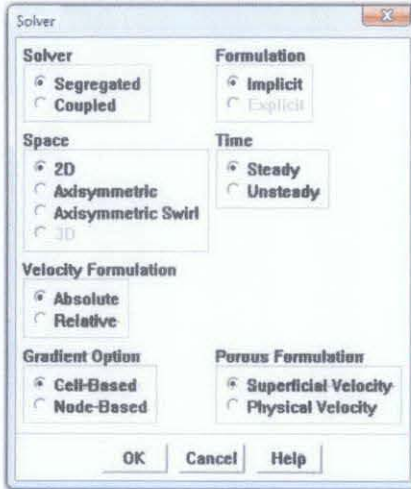
Define > Models > Viscous
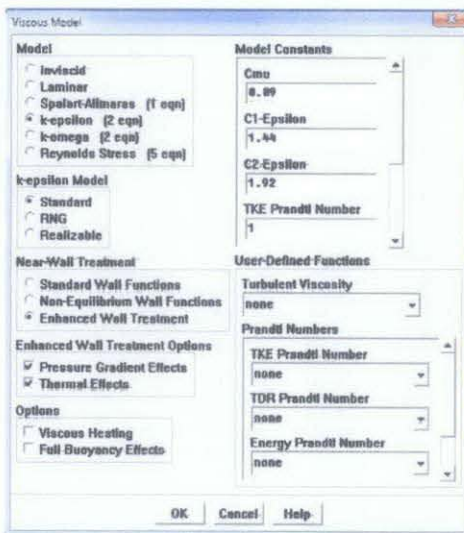
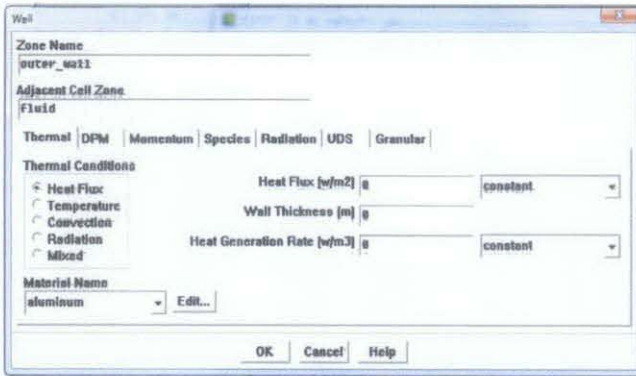Define > Models > Energy
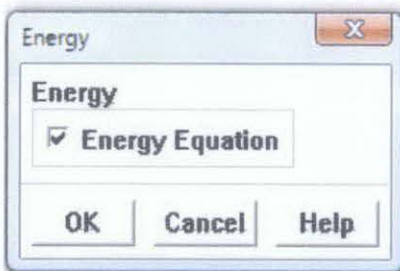
Define > Materials
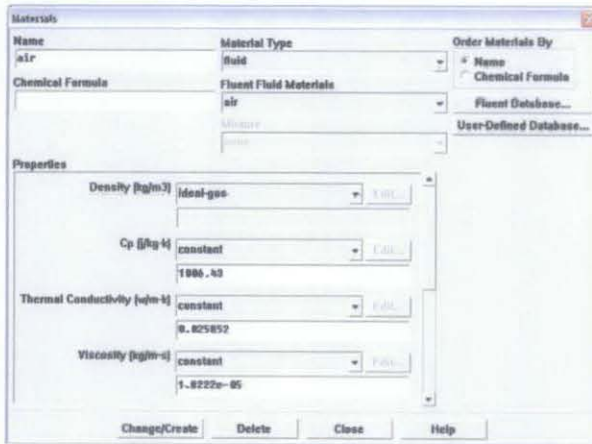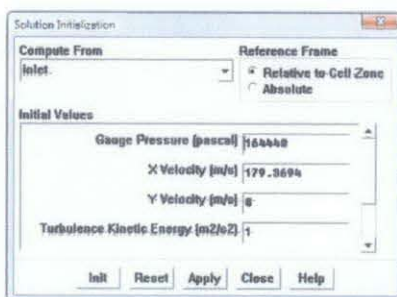

Define > Operating Conditions
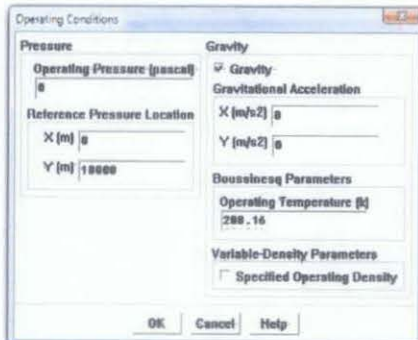
Define > Boundary Conditions
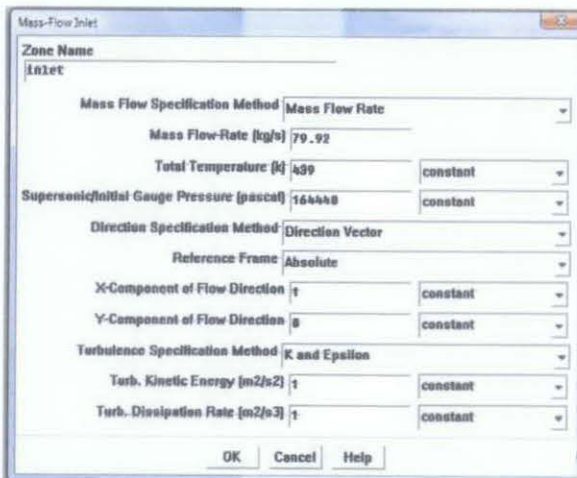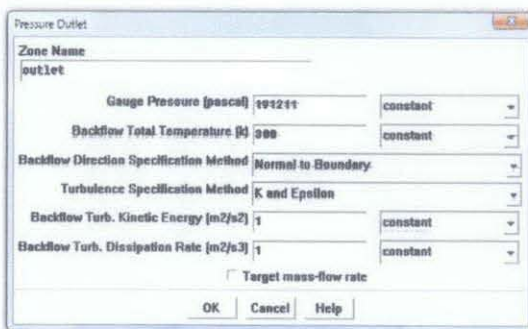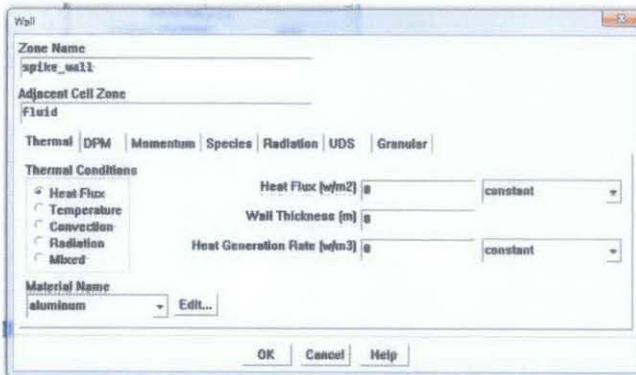
Solve > Initialize > Initialize...

Solve > Monitors > Residual...
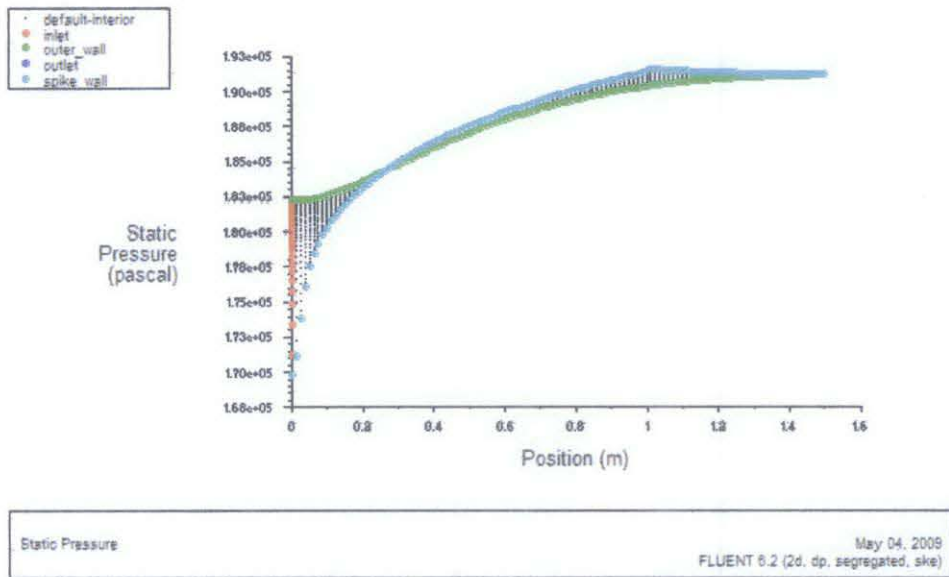
Main Menu > File > Write > Case File...
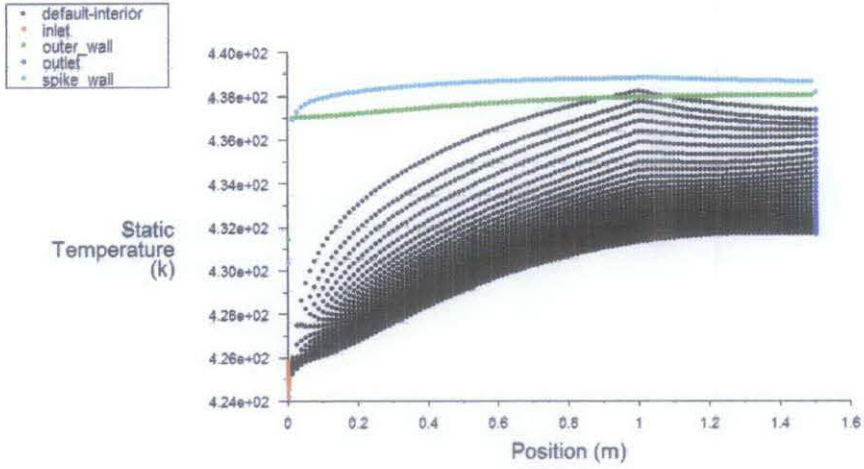
Solve > Iterate

Main Menu > File > Write > Data...

Save the solution to a data file after solution is converged

APPENDIX B: X-Y PLOT

The figures shown below are the X-Y plot for pressure, temperature and velocity done at Ma=2.2 and δ=6 and α=0 in the leeside.
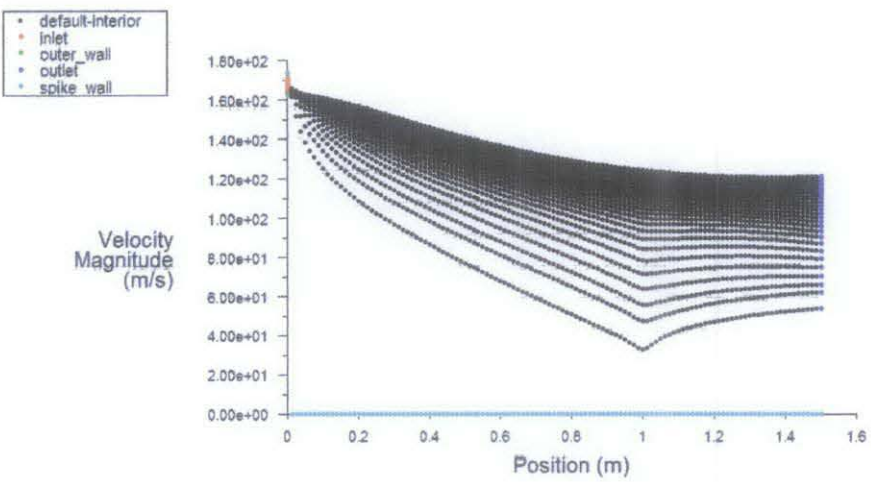

Pressure Distribution

Temperature Distribution

Velocity Distribution